NASA TECHNICAL NOTE

NASA TN D-3936

NASA TN D-3936

COMPARISON OF FLIGHT-MEASURED HELICOPTER ROTOR-BLADE CHORDWISE PRESSURE DISTRIBUTIONS WITH STATIC TWO-DIMENSIONAL AIRFOIL CHARACTERISTICS

by James Scheiman and Henry L. Kelley

Langley Research Center

Langley Station, Hampton, Va.

NATIONAL AERONAUTICS AND SPACE ADMINISTRATION • WASHINGTON, D. C. • MAY 1967

NASA TN D-3936

COMPARISON OF FLIGHT-MEASURED HELICOPTER ROTOR-BLADE CHORDWISE PRESSURE DISTRIBUTIONS WITH STATIC TWO-DIMENSIONAL AIRFOIL CHARACTERISTICS

By James Scheiman and Henry L. Kelley

Langley Research Center
Langley Station, Hampton, Va.

NATIONAL AERONAUTICS AND SPACE ADMINISTRATION

For sale by the Clearinghouse for Federal Scientific and Technical Information
Springfield, Virginia 22151 – CFSTI price $3.00

COMPARISON OF FLIGHT-MEASURED HELICOPTER ROTOR-BLADE CHORDWISE PRESSURE DISTRIBUTIONS WITH STATIC TWO-DIMENSIONAL AIRFOIL CHARACTERISTICS

By James Scheiman and Henry L. Kelley
Langley Research Center

SUMMARY

The blade section normal-force coefficients and centers of pressure of a helicopter rotor blade for two extreme flight conditions were compared with measured static two-dimensional airfoil characteristics. The two extreme flight conditions explored in detail were trim, level flights to obtain blade stall and high blade Mach numbers. Other trim-level-flight conditions were also studied.

A comparison of flight-measured characteristics and two-dimensional characteristics showed agreement over most of the rotor disk, but significant differences were found in certain regions on the rotor disk. These differences were largely confined to regions of high normal-force coefficients and, to a lesser degree, to regions at the advancing blade tip where Mach number effects were present. Possible causes of the differences are oscillating airfoil characteristics, preceding blade tip vortex effects, spanwise or yawed flow on the blade, and nonuniform velocity gradients ahead of the blade section.

INTRODUCTION

Rotor-blade dynamic loads are one of the major helicopter problems with respect to structural fatigue and acceptable fuselage vibration levels. The ability to predict these loads with reasonable accuracy has long been an objective of the helicopter industry. Assumptions which are entirely adequate for performance theory are not dependent upon a precise knowledge of rotor-blade loads. For an adequate structural dynamic analysis, however, a precise knowledge of the rotor-blade loads is necessary. One aspect of the airloads problem is the degree of validity of steady-state two-dimensional airfoil data to satisfactorily predict blade loads from calculated inflow velocities.

In the past, an absence of experimental information on periodic blade loading has been the major impediment to the derivation of a satisfactory airload-prediction theory and to the application of accurate limitations to the theory for trim-level-flight conditions. To help fill this gap, the National Aeronautics and Space Administration flight-tested a

single rotor helicopter equipped with extensive instrumentation which included numerous rotor-blade pressure transducers, motion pickups, and strain gages. With these flight data, a comparison can be made of the flight-measured and two-dimensional chordwise pressure distributions and the degree of validity of steady-state two-dimensional airfoil data to satisfactorily predict blade loads can be determined.

In this report, the blade section normal-force coefficients and centers of pressure for trim-level-flight conditions are discussed. Two trim-level-flight conditions are explored in detail to determine the effects of blade stall and Mach number. Normalized chordwise pressure distributions for these flights are presented. Other trim-level-flight conditions are sampled and the results are discussed. Portions of the data are compared with full-scale two-dimensional data by equating the two normal-force coefficients obtained at the same flight section Mach number. The specific purpose of this report is to compare the two-dimensional chordwise pressure distributions with the corresponding flight-measured distributions. The two-dimensional airfoil characteristics referred to herein are static two-dimensional characteristics as distinct from oscillating (unsteady) two-dimensional characteristics.

This study is an extension of the original work reported in reference 1.

SYMBOLS

The units used for the physical quantities defined in this section are given in both the U.S. Customary Units and in the International System of Units (SI). (See ref. 2.)

a	lift-curve slope
b	number of blades
c	blade section chord, inches (meters)
c_l	section lift coefficient
$\bar{c}_l$	mean section lift coefficient
C_N	normal-force coefficient, $\int_0^{1.0}\left(\frac{-\Delta p}{q}\right)d\left(\frac{x}{c}\right)$
I	mass moment of inertia of blade about flapping hinge, slug-feet^2 (kilogram-meters^2)
Δp	pressure difference between upper and lower surfaces of blade, pounds force/inch^2 (newtons/meter^2)

M blade section Mach number

q dynamic pressure, $\frac{1}{2}\rho U^2$, pounds force/inch^2 (newtons/meter^2)

r distance along blade-span axis measured from center of rotation, inches (meters)

R rotor-blade radius measured from center of rotation, inches (meters)

$U = \sqrt{U_T^{\,2} + U_P^{\,2}}$

U_P component at blade element of resultant velocity perpendicular both to blade span axis and U_T, feet/second (meters/second)

U_T component at blade element of resultant velocity perpendicular to blade span axis and to axis of no feathering, feet/second (meters/second)

V true airspeed of helicopter along flight path, feet/second (meters/second)

x distance along blade chord measured from leading edge, inches (meters)

x_{cp} chordwise distance from leading edge of blade to center of pressure, inches (meters)

α rotor-blade section angle of attack, degrees

α_s rotor angle of attack; angle between axis of no feathering (that is, axis about which there is no cyclic-pitch change) and plane perpendicular to flight path, positive when axis is inclined rearward, degrees

γ blade Lock number, $\frac{\rho acR^4}{I}$

ρ mass density of air, slugs/feet^3 (kilograms/meters^3)

μ rotor tip-speed ratio, $\frac{V \cos \alpha_s}{\Omega R}$

σ rotor solidity, $\frac{bc}{\pi R}$

ψ azimuth angle of rotor blade without any lagging motion, measured in direction of rotation from downwind position, degrees

Ω rotor angular velocity, radians/second

Subscripts:

max maximum

min minimum

APPARATUS

Test Helicopter

A photograph of the single rotor helicopter used in this investigation is presented as figure 1 and the pertinent helicopter characteristics are given in table I. The rotor system had four fully articulated blades with offset flapping and lagging hinges. The rotor was modified only to the extent necessary to instrument one blade. A full-span trailing-edge tab provided aerodynamic balance for the blade. The tab deflection was measured at the spanwise pressure stations $\frac{r}{R}$ and was found to have zero deflection except for a 4^{o} upward deflection at $\frac{r}{R} = 0.85$ and 0.90.

Instrumentation

Forty-nine pressure transducers were used in the test rotor blade to measure differential pressure. These transducers are the NASA miniature electrical pressure gages described in reference 3. Each gage measured the difference in pressure on the top and bottom surfaces of the blade. The gages were mounted in such a way that centrifugal force and flapping accelerations could not materially affect the accuracy of the gage output. To check these effects, the pressure orifices were sealed with tape and the rotor was operated. The location of the pressure orifices on the blade is shown in table II. The electrical output from all the pressure transducers was recorded simultaneously on oscillographs through a 160-contact slip-ring assembly. In addition, the slip rings permitted simultaneous recording of blade flapwise bending, chordwise bending, torsional moments, and the blade pitching, flapping, and lagging motions. The flight parameters were obtained by means of standard NASA recording instruments having synchronized time scales.

DATA REDUCTION AND ACCURACY

Flight Data

Each pressure data point used is an average of three oscillograph data points recorded in three consecutive rotor revolutions. Selected portions of the oscillograph film were read and transcribed to punch cards by the use of semiautomatic film reading equipment. These cards were then processed through an electronic digital computer and the final results tabulated. Questionable data points were checked by hand reading.

An analysis of the overall system errors indicated that the largest errors in the data were introduced during the actual reading of the time histories. The reading accuracy of each data point is highly dependent upon the amplitude, frequency, and the repeatability of the oscillograph trace. The high-amplitude, high-frequency records were the most difficult to read. The estimated reading accuracy of the difficult-to-read data points is ±3 percent with 99.7 percent confidence and ±2 percent with 95 percent confidence. A more detailed discussion of the data reduction, accuracy, and dynamic gage characteristics may be obtained from reference 4.

Static Two-Dimensional Data

The two-dimensional airfoil characteristic data used for comparison with flight results are presented in reference 5. The tunnel test model was an untwisted full-scale section of the helicopter rotor blade instrumented with pressure gages at 15 chordwise stations. The span was 32.70 in. (83.06 cm). The tests were conducted over a Mach number range from 0.3 to 0.8 and a corresponding Reynolds number range from 1.4×10^6 to 3.8×10^6. The corrected section angle of attack varied from -4° to 26° for a Mach number of 0.3 and from -4° to 5° for a Mach number of 0.8. Tunnel tests were performed on a section with a 0° tab deflection and a section with a 3° tab deflection.

Method of Comparison of Flight and Two-Dimensional Chordwise Pressure Distributions

The flight and wind-tunnel chordwise pressure distributions are compared on the basis of equal normal-force coefficients $\left(\text{equal areas under the curves of } \frac{\Delta p}{q} \text{ as a function of } \frac{x}{c}\right)$ and equal Mach numbers. Thus, the comparison is independent of actual section angle of attack. The normal-force coefficients were determined by dividing the blade section loading by the respective dynamic pressure of the coefficients. The flight dynamic pressure was determined from the velocity U which was computed by assuming a rigid blade and a uniform inflow that was compatible with the test helicopter lift and drag requirements. Figure 2 is a diagram of the rotor blade element in forward flight and

shows the pertinent angles and velocities relative to the control axis. The blade section loading flight data were determined by numerical integration of the differential pressure data.

Since the blade is a modified NACA 0012 section and the two-dimensional wind-tunnel test data are limited to a minimum Mach number of 0.3, it was assumed that the two-dimensional pressure distributions were constant between $0.15 \leqq M \leqq 0.3$ and that the two-dimensional normal-force coefficients were constant between $0.08 \leqq M \leqq 0.3$ and were the same as those for $M = 0.3$.

PRESENTATION OF CHORDWISE PRESSURE DATA

The chordwise pressure distributions for the two flight conditions are presented in figures 3 and 4. For comparison purposes, a sample of the two-dimensional pressure distributions is presented in figure 5. These pressure distributions are normalized by dividing by the respective normal-force coefficients.

Flight To Obtain Blade Stall

The normalized chordwise pressure distributions for the flight condition to obtain blade stall are presented in figure 3. This flight was made with a near-minimum rotor rotational speed of 193 rpm and a tip-speed ratio of 0.23 and was performed with the expectation of producing local blade section stalling. The advancing blade tip Mach number was 0.64. Because of the proximity to the reversed-velocity region boundary (zero q), three of the plots are blank. A tabulation of the flight data used to obtain figure 3 is available in table IV of reference 6.

Flight To Obtain High Blade Mach Numbers

A tabulation of the flight test data used to obtain the normalized chordwise pressure distributions in figure 4 is available in table 20 of reference 4. This flight was made to obtain high advancing blade tip Mach numbers by operating at a near maximum rotor rotational speed of 246 rpm with a tip-speed ratio of 0.25. The advancing blade tip Mach number was 0.9.

Sample Two-Dimensional Wind-Tunnel Data

A sample of the static normalized two-dimensional wind-tunnel chordwise pressure distributions obtained from reference 5 is presented in figure 5. The normal-force coefficients for these data were determined by mechanical integration of the area under the respective curves of $\frac{\Delta p}{q}$ as a function of $\frac{x}{c}$.

ANALYSIS AND DISCUSSION

The results are presented and discussed in three sections: (1) normal-force coefficients, (2) sample chordwise pressure distributions, and (3) chordwise centers of pressure. The rotor areas considered were not carried inboard of $\frac{r}{R} = 0.40$ to avoid areas of the disk with low dynamic pressures. Also, rotor areas outboard of $\frac{r}{R} = 0.95$ were not considered because of uncertainties created by the presence of the blade tip. The comparisons of all pertinent flight and static airfoil data are presented. This presentation is followed by a discussion of possible reasons for differences in the data.

Normal-Force Coefficients

The normal-force coefficients for the two trim-level-flight conditions (flight to obtain blade stall and flight to obtain high blade Mach numbers) are presented as contour plots in figures 6 and 7. For convenience, a plot of normal-force coefficient as a function of angle of attack, based on two-dimensional wind-tunnel tests (refs. 5 and 7), is provided in figure 8. In this figure the normal-force coefficients from reference 4 were obtained by mechanical integration of the curve of $\frac{\Delta p}{q}$ as a function of $\frac{x}{c}$.

Flight to obtain blade stall.- The normal-force coefficients for the flight to obtain blade stall are presented in figure 6. Note that some of the normal-force coefficients are above those predicted from two-dimensional data (see fig. 8 where the maximum unstalled C_N is 1.30).

Figure 9 indicates areas on the rotor where flight and two-dimensional chordwise pressure distributions differ. This plot is for the same flight condition presented in figures 3 and 6. The dotted region in figure 9 indicates the area where the flight normal-force coefficients are above the two-dimensional stall value ($C_N > 1.30$). The checkered region in figure 9 indicates the area on the rotor where the flight and two-dimensional chordwise pressure distributions differ.

Mach number divergence can be encountered on the retreating side of the rotor at relatively low Mach numbers if the section angle of attack is high enough. Therefore, the standard NACA definition of lift and drag divergence (ref. 8) was applied to this flight for the area of disagreement shown in figure 9, and no divergence was indicated. Also shown in this figure is the tip path of the preceding blade (90° ahead of the instrumented blade) which gives an approximate location of the resulting leading blade tip vortex. The tip vortex is known to produce a strong contribution to the nonuniformities of inflow (ref. 6).

Flight to obtain high blade Mach numbers.- The normal-force coefficients from the flight to obtain high blade Mach numbers are presented in figure 7. Figure 10 indicates

areas on the rotor where flight and two-dimensional chordwise pressure distributions do not agree.

A Mach number divergence analysis was made of the advancing side of the rotor. In figure 10, lift divergence was indicated over a rotor area slightly smaller than the area showing differences between flight and two-dimensional pressure distributions. Linear interpolation was used for the high Mach numbers to obtain the two-dimensional pressure distributions. Lift divergence in the same area as the disagreement in distributions suggests the possibility that the linear interpolation technique used at the high Mach numbers may have been inadequate and may have actually introduced the disagreement noted. It should also be noted that the area of chordwise pressure disagreement concerns only the shape of the chordwise distributions and that the presence of this area does not necessarily indicate whether Mach number effects are more, or less, serious than would be predicted from two-dimensional data.

Sample Chordwise Pressure Distributions

Flight-measured pressure distributions are compared with the corresponding two-dimensional pressure distributions in figures 11 and 12. The associated two-dimensional section angles of attack determined by linear interpolation are also indicated in the figures. When more than one two-dimensional curve was possible, they are presented. When the flight C_N value was greater than the unstalled two-dimensional C_N value, no two-dimensional data are presented. The azimuth position and radial station at which the comparisons in figures 11 and 12 are made are indicated by symbols on the C_N contour plots of figures 6 and 7, respectively.

Flight to obtain blade stall.- The samples of chordwise pressure distributions, shown in figure 11, are from the flight where blade section stalling was expected. The rotor areas where flight and two-dimensional pressure distributions differ in figure 9 can be separated into three distinct regions: (1) the area where the flight $C_N > 1.3$ and the pressure distribution is similar to that of an unstalled two-dimensional section, (2) the area where the flight $C_N > 1.3$ and the pressure distribution has no comparable two-dimensional distribution, and (3) the area where the flight $C_N < 1.3$ and there is no comparable two-dimensional pressure distribution. Samples of the pressure distribution for the first area are shown in figure 11(a) at $\psi = 195^o$ and in figure 11(b) at $\psi = 210^o$, 225^o, and 240^o. Typical pressure distributions for the second area are shown in figure 11(a) at $\psi = 210^o$, 225^o, 240^o, and 255^o and those for the third area are shown in figure 11(a) at $\psi = 270^o$ and in figure 11(b) at $\psi = 270^o$ and 285^o.

The flight-measured pressure distribution shown by the circles in figure 11(d) is typical of that of a stalled section. The correlation with the two-dimensional data shown in figure 11(d) at angles of attack in the vicinity of stall is only fair.

Flight to obtain high blade Mach numbers.- Samples of the chordwise pressure distributions, shown in figure 12, are from the flight where blade Mach number effects were expected. In figure 12(c) from $\psi = 30^{\circ}$ to 135° is the region in which the flight $C_N < 1.3$ but for which there is no comparable two-dimensional pressure distribution. However, this region is in an area where lift divergence is indicated and linear Mach number interpolation of two-dimensional data is expected to introduce errors.

Centers of Pressure

Differences between flight and two-dimensional airfoil characteristics discussed previously also have an influence on the prediction of section aerodynamic pitching moments. The variation of two-dimensional center of pressure with section angle of attack is shown in figure 8, where the centers of pressure from reference 5 are based on the external balance measurements.

Figures 13 and 14 present blade section center-of-pressure contour plots determined from flight data. Center-of-pressure data inboard of $\frac{r}{R} = 0.40$ and outboard of $\frac{r}{R} = 0.95$ are not shown because of the low dynamic pressures and tip effects, respectively.

Flight to obtain blade stall.- Contour plots of the center of pressure for flight with expected blade stall are presented in figure 13. Lines of constant centers of pressure are shown in figure 13(a). Areas are indicated in figure 13(b) where the center of pressure is forward of the 21-percent-chord point and aft of the 30-percent-chord point. It should be noted in figure 8 that centers of pressure for two-dimensional data do not move forward of the 21-percent-chord point and that angles of attack above 14° are required to obtain centers of pressure aft of the 30-percent-chord point. Typical chordwise pressure distributions for the rotor area with the center of pressure aft of the 30-percent-chord point can be seen in figure 11(a) from $\psi = 210^{\circ}$ to 270° and in figure 11(b) at $\psi = 270^{\circ}$ and 285°. Typical chordwise pressure distributions with center of pressure forward of the 21-percent-chord point can be seen in figure 11(c) from $\psi = 60^{\circ}$ to 120°. Even though these centers of pressure are farther forward than those for the two-dimensional data, the chordwise pressure distributions, as such, were judged to have reasonable agreement.

Flight to obtain high blade Mach numbers.- Contour plots of the center of pressure for flight to obtain high blade Mach numbers are presented in figure 14. Lines of constant center of pressure are shown in figure 14(a). Areas of the rotor where the center of pressure is forward of the 21-percent-chord point and aft of the 30-percent-chord point are

indicated in figure 14(b). Typical chordwise pressure distributions with the center of pressure forward of the 21-percent-chord point can be seen in figure 12(c) from $\psi = 30^{\circ}$ to 135°.

Other Trim-Level-Flight Conditions

A less thorough study of several other trim-level-flight conditions was made to explore rotor areas where the flight normal-force coefficients were greater than the two-dimensional stall values. The results for six flight conditions, all of which have a tip-speed ratio greater than 0.2, are shown in figure 15. These plots are listed in the order of increasing forward speed and decreasing mean lift coefficient. The dotted areas shown in figure 15 correspond to the areas of two-dimensional chordwise pressure disagreement described by the dotted areas in figure 9, namely where $C_N > 1.3$. Also shown is the area where $C_N > 1.6$. For all conditions presented, this area of disagreement is in the third rotor azimuth quadrant and includes the preceding blade-tip-vortex trajectory. Other trim-level-flight conditions for a tip-speed ratio of less than 0.2 were plotted and all normal-force coefficients were found to be less than 1.3.

Probable Factors Affecting Correlation

It has been shown from flight measurements that the pressure distributions over a portion of the rotor disk do not agree with the corresponding two-dimensional airfoil pressure distributions for the specific flight conditions studied. Even though a complete explanation for these differences is not available at the present time, a discussion of some probable causes is desirable.

The airfoil characteristics of a two-dimensional airfoil oscillating in pitch have been available for many years. (See refs. 9 to 14.) High rates of change of angle of attack are known to increase the unstalled angle of attack to values above the two-dimensional stall value. This effect can be seen in figure 16. Although the peak-to-peak two-dimensional values of C_N for an oscillating airfoil do not agree with static two-dimensional data, there is usually no net gain in the mean C_N between $C_{N,max}$ and $C_{N,min}$; therefore, this effect is not expected to have any significant effect on rotor performance calculations. An example of the high rate of change in angle of attack from flight data can be seen in figure 6. Between $\frac{r}{R} = 0.55$ and 0.75 and $\psi = 180^{\circ}$ and 210°, the rate of increase in angle of attack is estimated to be about 100° per second or 1° per $2\frac{1}{2}$ blade chords based on the measured rate of change in normal-force coefficient.

At present, it is believed that in the regions in which $C_N > 1.3$ and the pressure distribution is similar to that of an unstalled two-dimensional section the difference can be attributed to rapid increases in angle of attack. In rotor regions where there are no comparable two-dimensional pressure distributions, regardless of the magnitude of C_N,

the difference is probably being introduced by airfoil characteristics like those found on the back side of the "hysteresis loop" and resulted from oscillating airfoil effects. However, a positive conclusion is not possible because of an insufficiency of chordwise pressure distribution data for oscillating airfoils. The rapid increase in angle of attack can be attributed, at least in part, to pitch-angle change and/or inflow-velocity changes that can be caused by the tip vortex of a preceding blade. The path of the tip of the preceding blade, which represents the approximate location of the tip vortex, is shown in figures 9, 10, and 15. The location of the tip vortex relative to the areas of high C_N indicates that tip vortex effects may be present.

In figure 9 the path of the tip of the preceding blade (approximate tip vortex location) crosses the blade section path at $\frac{r}{R} = 0.85$ and at $\psi \approx 110^o$. It can be seen in figure 3 for $\frac{r}{R} = 0.85$ that the normalized chordwise pressure distribution has a minor distortion from $\psi = 90^o$ to 120^o. Also, in figure 9 the preceding blade tip path crosses $\frac{r}{R} = 0.75$ at $\psi \approx 130^o$ and becomes tangent to $\frac{r}{R} = 0.55$ at $\psi \approx 205^o$. An example of the effect of the tip vortex is shown in the flight data of figure 3; for $\frac{r}{R} = 0.75$ the most forward chordwise pressure gage indicates a decrease in pressure from $\psi = 105^o$ to 180^o and from $\psi = 255^o$ to 330^o. These regions are in proximity to the path of the preceding blade tip. Also, at $\frac{r}{R} = 0.55$ the pressure distributions are greatly distorted from $\psi = 210^o$ to about 345^o.

Because of compressibility effects on the advancing blade during high Mach number flight, the tip vortex effect is more complex. In figure 10 the preceding blade tip path crosses $\frac{r}{R} = 0.85$ at $\psi \approx 105^o$; the normalized chordwise pressure distribution is distorted in figure 4 at $\frac{r}{R} = 0.85$ from $\psi = 75^o$ to 150^o. It is also interesting to note the flight-measured normalized pressure distribution in the neighborhood of the reversed-velocity region (fig. 4 at $\frac{r}{R} = 0.25$ from $\psi = 240^o$ to 315^o). Examination of pressure data at higher μ values indicates similar pressure distributions just inside the reversed-velocity region (see, for example, ref. 4, table 16, 17, 18, 19, 21, 22, or 23).

Another cause of the differences in flight and two-dimensional airfoil characteristics is the spanwise forces acting on the boundary layer. Typical examples of this phenomenon, obtained from swept-wing tests, can be found in references 15 to 19. Another example, as found in propeller studies (ref. 20), indicated that measured blade-root maximum normal-force coefficients were found to be larger than the maximum static two-dimensional values. There are undoubtedly other influencing factors such as shed vortices and nonuniform velocities ahead of the airfoil (ref. 21).

The differences in flight and two-dimensional airfoil characteristics are reflected in blade loads. A hysteresis loop would be expected to increase the magnitude of vibratory forces acting on the blade over those predicted by using static two-dimensional data.

However, the resulting effects on the vibratory blade moments or stresses will vary with details of the aerodynamic distributions over the flexible blade. A specific example where the hysteresis loop did cause a substantial increase in calculated flap bending moments is presented in reference 22.

CONCLUDING REMARKS

Chordwise pressure distributions measured in flight on a helicopter rotor blade are compared with corresponding two-dimensional airfoil data. Although agreement is the rule rather than the exception, significant differences were found in certain regions on the rotor disk. In addition, a comparison of the experimentally determined local normal-force coefficients and centers of pressure with two-dimensional wind-tunnel data indicates some differences for rotor tip-speed ratios greater than 0.2. Oscillating airfoil characteristics, preceding blade tip vortex effects, spanwise or yawed flow on the blade, and nonuniform velocity gradients ahead of the blade section are possible causes of the differences. These differences will influence both vibratory blade flapping moments and control system loads predicted from two-dimensional data and uniform inflow calculations.

Langley Research Center,
National Aeronautics and Space Administration,
Langley Station, Hampton, Va., December 16, 1966,
721-01-00-29-23.

REFERENCES

1. Scheiman, James; and Kelley, Henry L.: Comparison of Flight Measured Helicopter Rotor Blade Chordwise Pressure Distributions and Two-Dimensional Airfoil Characteristics. CAL/TRECOM Symposium Proceedings Vol I – Dynamic Load Problems Associated With Helicopters and V/STOL Aircraft, June 1963.

2. Mechtly, E. A.: The International System of Units – Physical Constants and Conversion Factors. NASA SP-7012, 1964.

3. Patterson, John L.: A Miniature Electrical Pressure Gage Utilizing a Stretched Flat Diaphragm. NACA TN 2659, 1952.

4. Scheiman, James: A Tabulation of Helicopter Rotor-Blade Differential Pressures, Stresses, and Motions as Measured in Flight. NASA TM X-952, 1964.

5. Lizak, Alfred A.: Two-Dimensional Wind-Tunnel Tests of an H-34 Main Rotor Airfoil Section. TREC Tech. Rept. 60-53 (SER-58304), U.S. Army Transportation Res. Command (Fort Eustis, Va.), Sept. 1960.

6. Scheiman, James; and Ludi, LeRoy H.: Qualitative Evaluation of Effect of Helicopter Rotor-Blade Tip Vortex on Blade Airloads. NASA TN D-1637, 1963.

7. Critzos, Chris C.; Heyson, Harry H.; and Boswinkle, Robert W., Jr.: Aerodynamic Characteristics of NACA 0012 Airfoil Section at Angles of Attack From 0^{o} to 180^{o}. NACA TN 3361, 1955.

8. Graham, Donald J.; Nitzberg, Gerald E.; and Olson, Robert N.: A Systematic Investigation of Pressure Distributions at High Speeds Over Five Representative NACA Low-Drag and Conventional Airfoil Sections. NACA Rept. 832, 1945.

9. Rainey, A. Gerald: Measurement of Aerodynamic Forces for Various Mean Angles of Attack on an Airfoil Oscillating in Pitch and on Two Finite-Span Wings Oscillating in Bending With Emphasis on Damping in the Stall. NACA Rept. 1305, 1957. (Supersedes NACA TN 3643.)

10. Silverstein, Abe; and Joyner, Upshur T.: Experimental Verification of the Theory of Oscillating Airfoils. NACA Rept. 673, 1939.

11. Halfman, Robert L.; Johnson, H. C.; and Haley, S. M.: Evaluation of High-Angle-of-Attack Aerodynamic-Derivative Data and Stall-Flutter Prediction Techniques. NACA TN 2533, 1951.

12. Harper, Paul W.; and Flanigan, Roy E.: Investigation of the Variation of Maximum Lift for a Pitching Airplane Model and Comparison With Flight Results. NACA TN 1734, 1948.

13. Harper, Paul W.; and Flanigan, Roy E.: The Effect of Rate of Change of Angle of Attack on the Maximum Lift of a Small Model. NACA TN 2061, 1950.

14. Moore, Franklin K.: Lift Hysteresis at Stall as an Unsteady Boundary-Layer Phenomenon. NACA Rept. 1291, 1956. (Supersedes NACA TN 3571.)

15. Tunnel Staff of Aero. Dept.; and Brebner, G. G.: Pressure and Boundary Layer Measurements on a 59° Sweptback Wing at Low Speed and Comparison With High Speed Results on a 45° Swept Wing. C.P. No. 86, Brit. A.R.C., 1952.

16. Garner, H. C.; and Walshe, D. E.: Pressure Distribution and Surface Flow on 5% and 9% Thick Wings With Curved Tip and 60° Sweepback. R. & M. No. 3244, Brit. A.R.C., 1962.

17. Black, Joseph: Pressure Distribution and Boundary Layer Investigations on a 44° Sweptback Tapered Wing. C.P. No. 137, Brit. A.R.C., 1953.

18. Garner, H. C.; and Bryer, D. W.: Experimental Study of Surface Flow and Part-Span Vortex Layers on a Cropped Arrowhead Wing. R. & M. No. 3107, Brit. A.R.C., 1959.

19. Hall, I. M.; and Rogers, E. W. E.: Part I – The Flow Pattern on a Tapered Sweptback Wing at Mach Numbers Between 0.6 and 1.6. Part II – Experiments With a Tapered Sweptback Wing of Warren 12 Planform at Mach Numbers Between 0.6 and 1.6. R. & M. No. 3271, Brit. A.R.C., 1962.

20. Himmelskamp, H.: Profile Investigations on a Rotating Airscrew. Rept. Transl. No. 832, Brit. M.A.P. Völkenrode, Sept. 1, 1947.

21. Vidal, R. J.; Curtis, James T.; and Hilton, J. H.: The Influence of Two-Dimensional Stream Shear on Airfoil Maximum Lift. TCREC Tech. Rept. 61-93 (Cornell Aeron. Lab. Rept. No. A1-1190-A-7), U.S. Army Transportation Res. Command (Fort Eustis, Va.), Aug. 1961.

22. LaForge, S. V.: Effects of Blade Stall on Helicopter Rotor Blade Bending and Torsional Loads. Rept. 347-V-1002 (HTC-AD 64-8) (Contract NOw-0422-c), Hughes Tool Co., May 1, 1965. (Available from DDC as AD 619713.)

TABLE I.- PRINCIPAL DIMENSIONS AND APPROXIMATE PHYSICAL CHARACTERISTICS OF TEST HELICOPTER AND ROTOR

Test weight, lbf (N)	Between 11 805 (52 511) and 11 200 (49 820)
Number of blades	4
Rotor blade radius, ft (m)	28 (8.5)
Flapping-hinge offset, ft (m)	1.0 (0.30)
Weight per blade (approximate), lbf (N)	175 (778.44)
Main rotor blade:	
Type	All metal, constant chord
Twist, deg	-8
Airfoil section	Modified NACA 0012
Blade chord, ft (m)	1.367 (0.4167)
Rotor solidity, σ	0.0622
Rotor-blade Lock number (approximate), γ	9.7
Normal rotor-blade tip speed, ft/sec (m/sec)	623 (190)
Normal rotor angular velocity, rad/sec	22.2
Test disk loading, lbf/sq ft (N/m^2)	4.79 (229)
Mass moment of inertia of blade about flapping hinge, slug-ft^2 (kg-m^2)	1176 (1594)
Forward rotor shaft tilt, deg	3.0

TABLE II.- FLIGHT CHORDWISE PRESSURE-ORIFICE LOCATIONS

x/c at –						
r/R = 0.25	r/R = 0.40	r/R = 0.55	r/R = 0.75	r/R = 0.85	r/R = 0.90	r/R = 0.95
0.042	0.042	0.017	0.017	0.017	0.017	0.017
.158	.158	.090	.090	.040	.090	.090
.300	.300	.168	.169	.090	.168	.168
.600	.600	.233	.233	.130	.233	.233
.910	.910	.335	.335	.168	.335	.335
		.625	.625	.233	.625	.625
		.915	.915	.335	.915	.915
				.500		
				.625		
				.769		
				.915		

Figure 1.- Test helicopter. L-61-4198

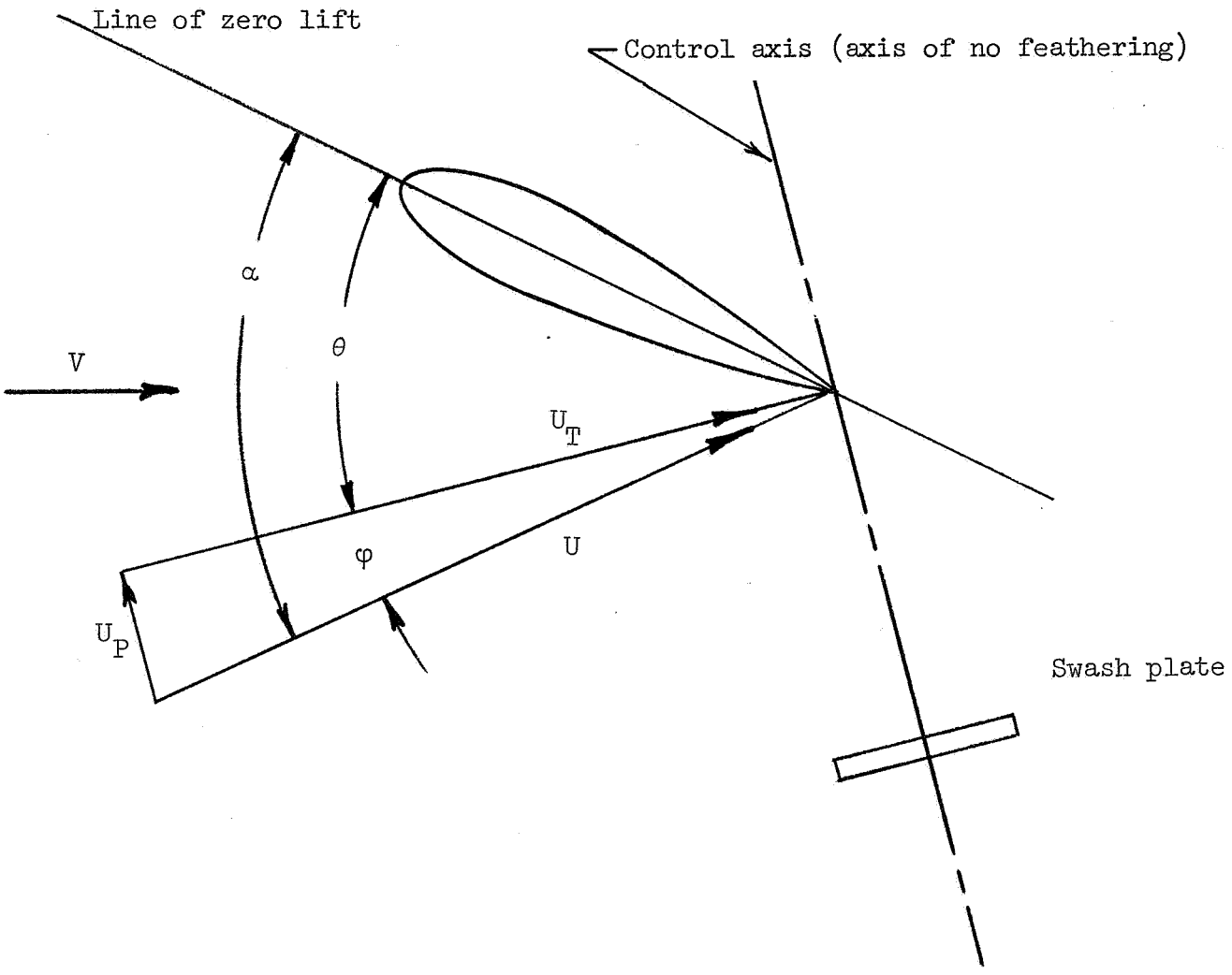

Figure 2.- Diagram of rotor-blade element in forward flight showing angles and velocities relative to the control axis.

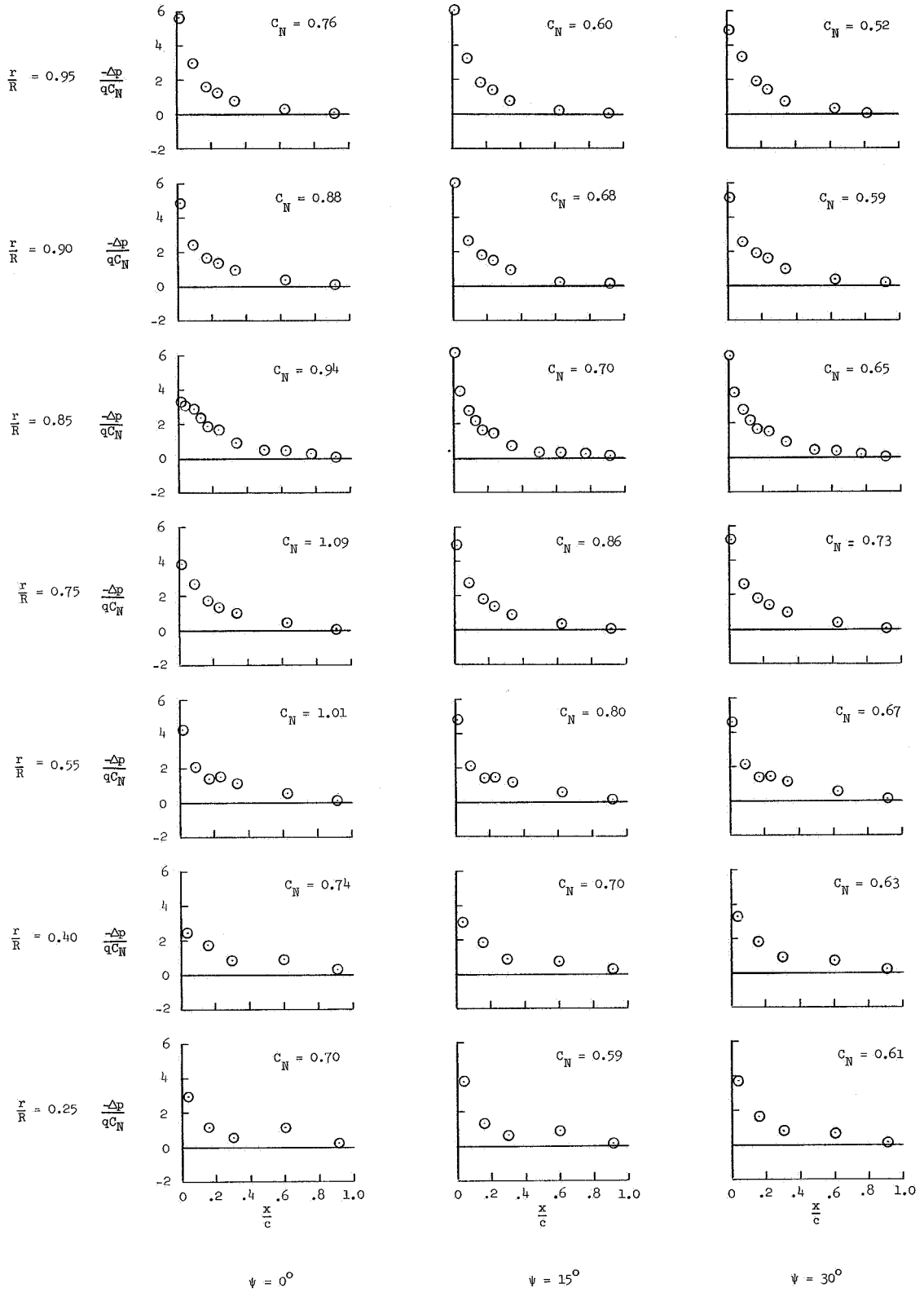

Figure 3.- Normalized chordwise pressure distributions for flight to obtain blade stall.

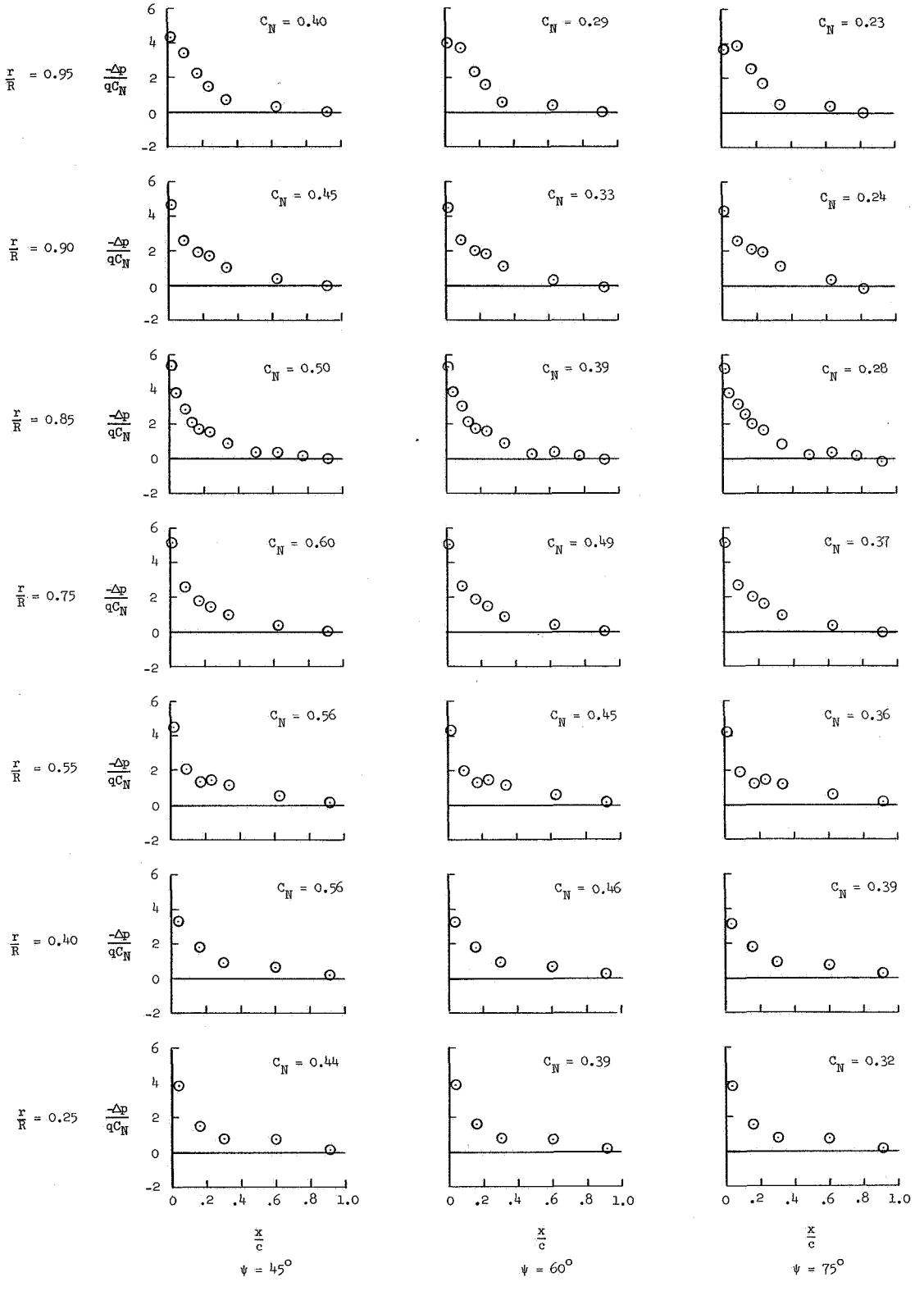

Figure 3.- Continued.

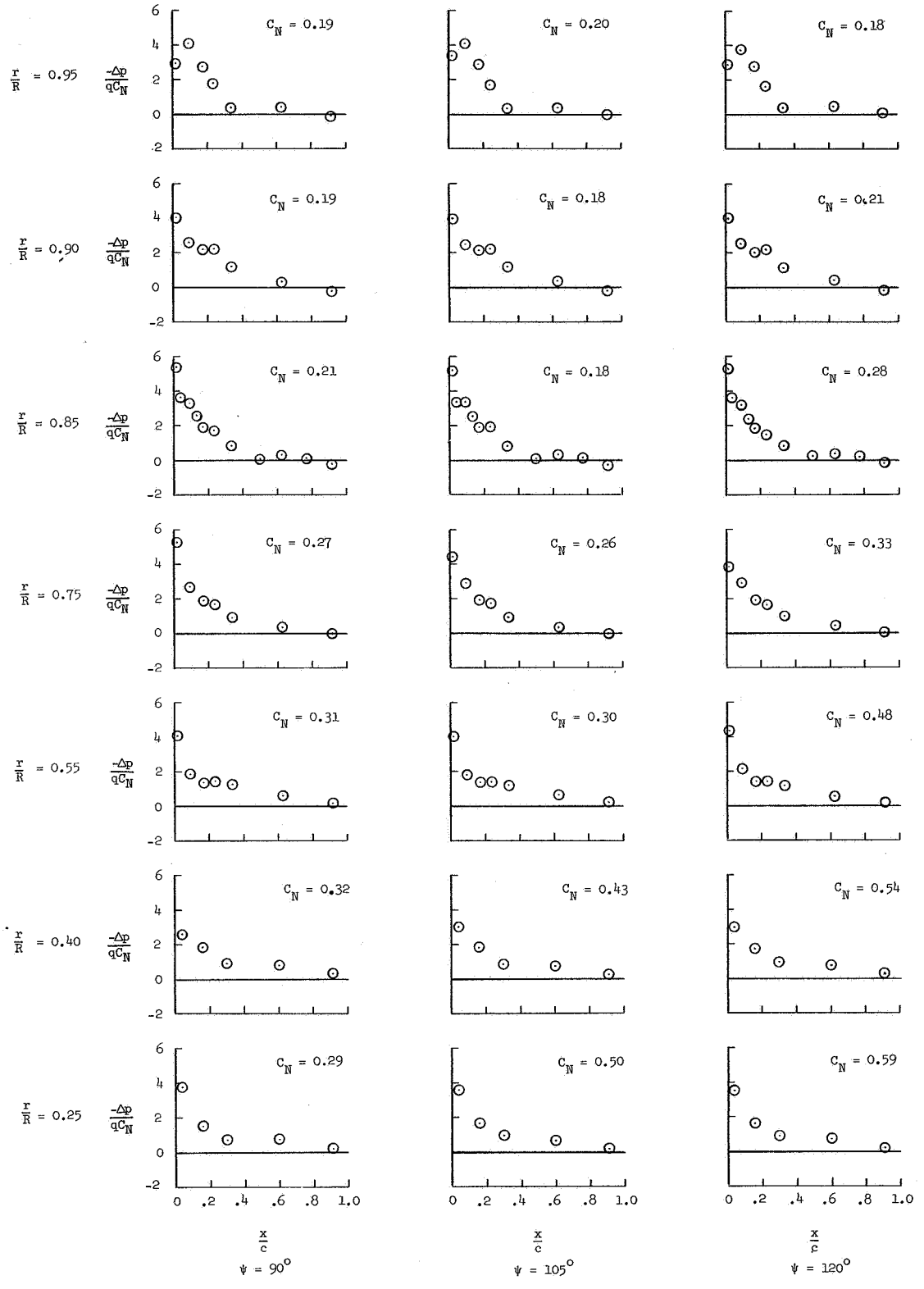

Figure 3.- Continued.

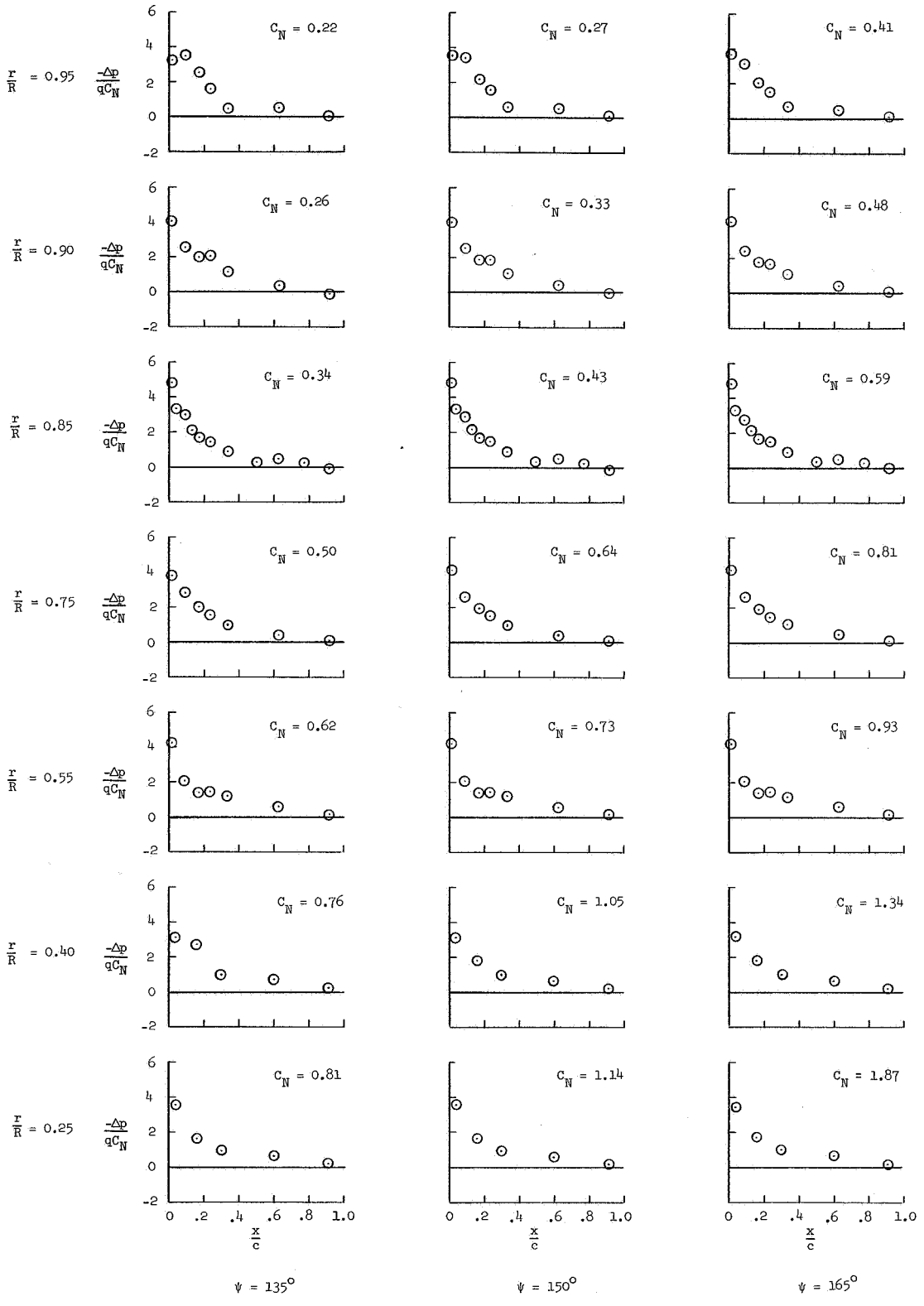

Figure 3.- Continued.

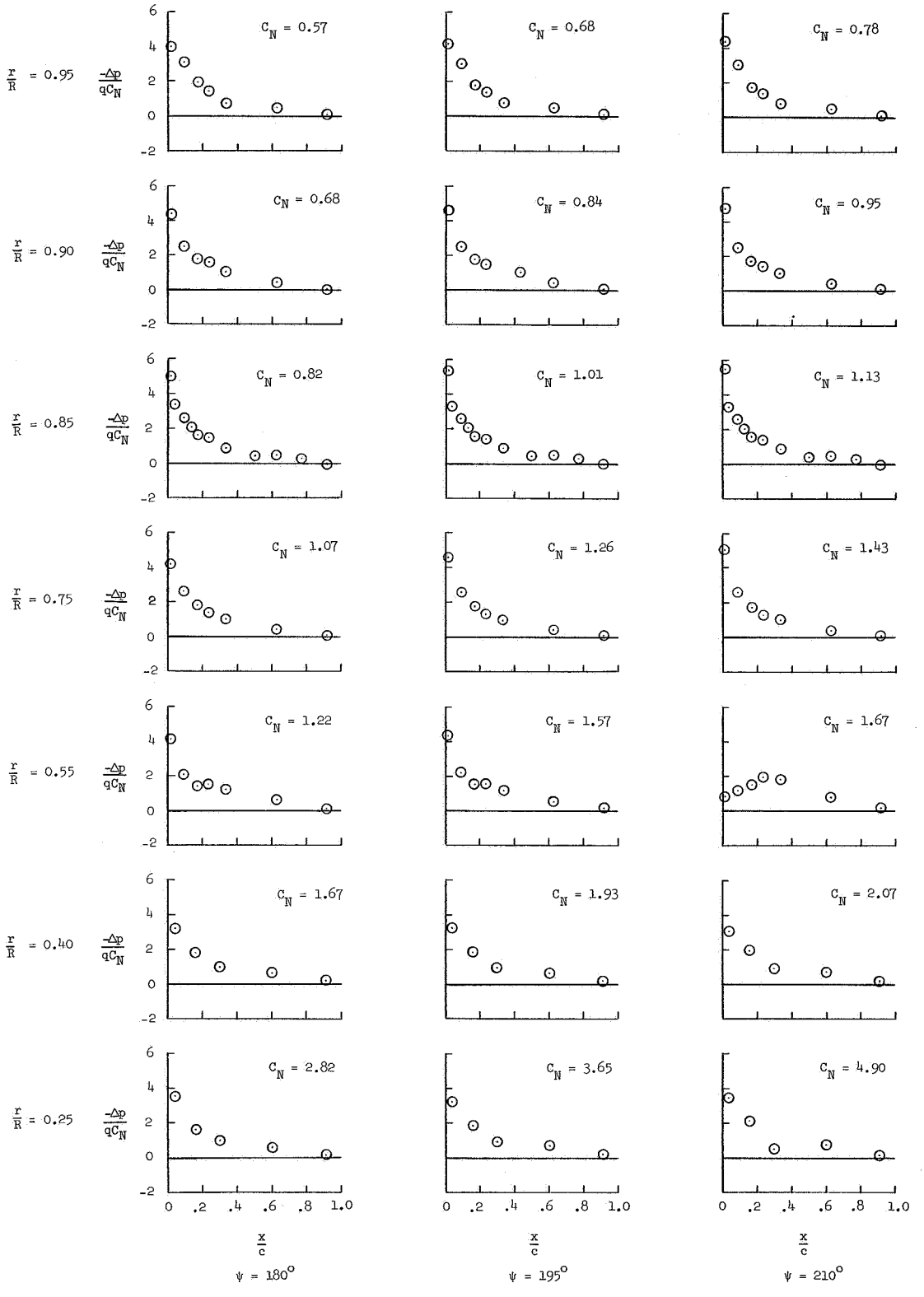

Figure 3.- Continued.

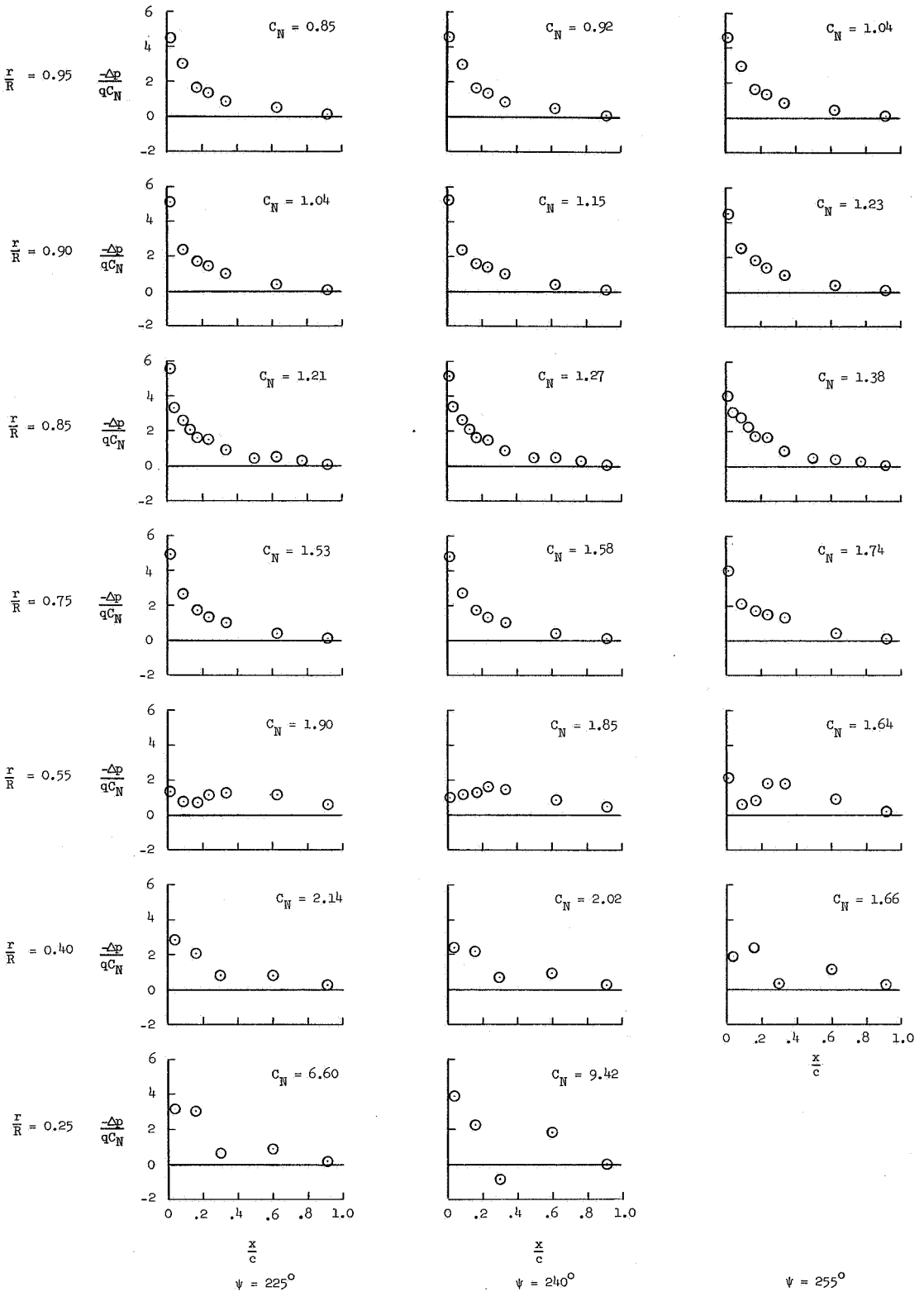

Figure 3.- Continued.

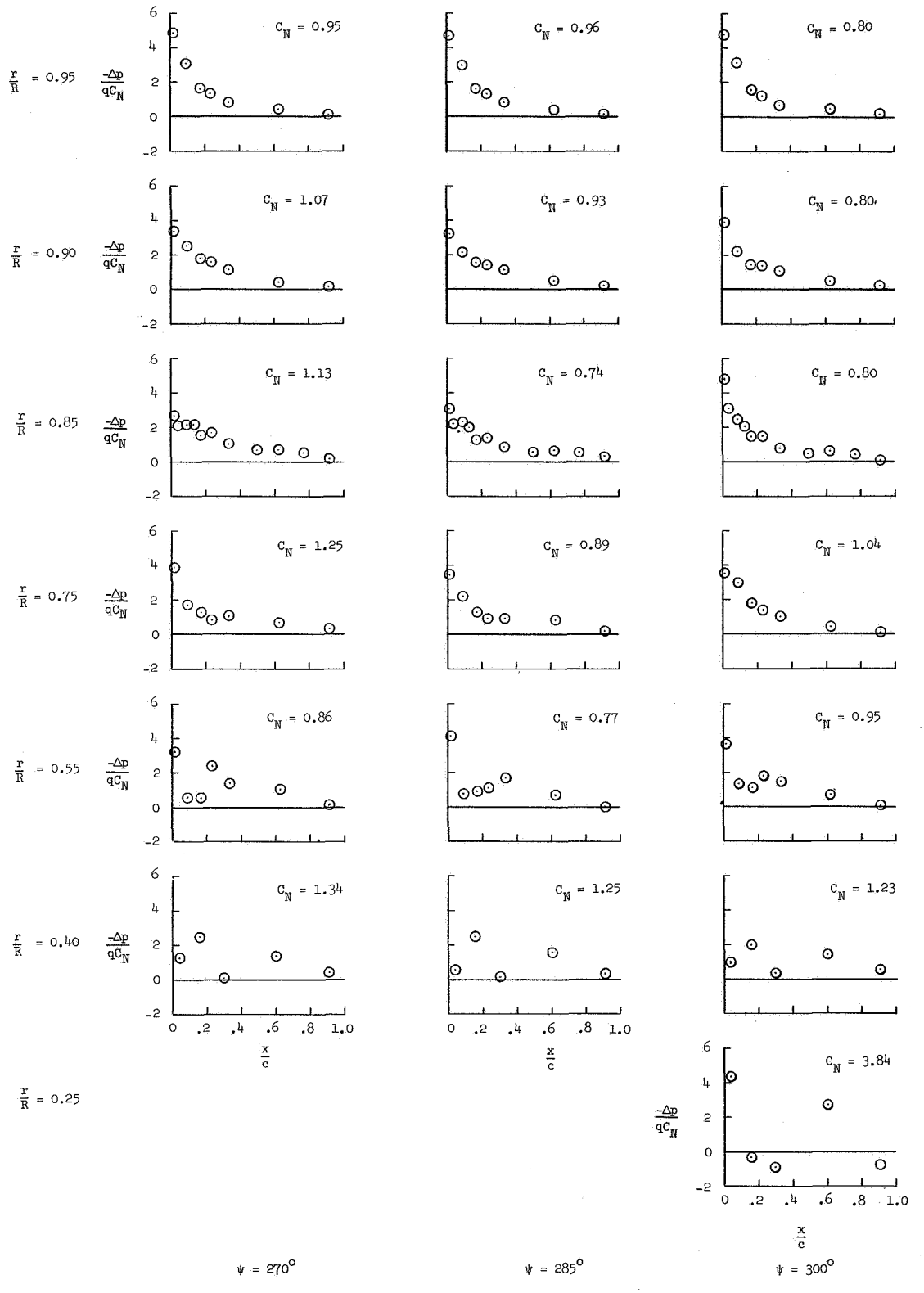

Figure 3.- Continued.

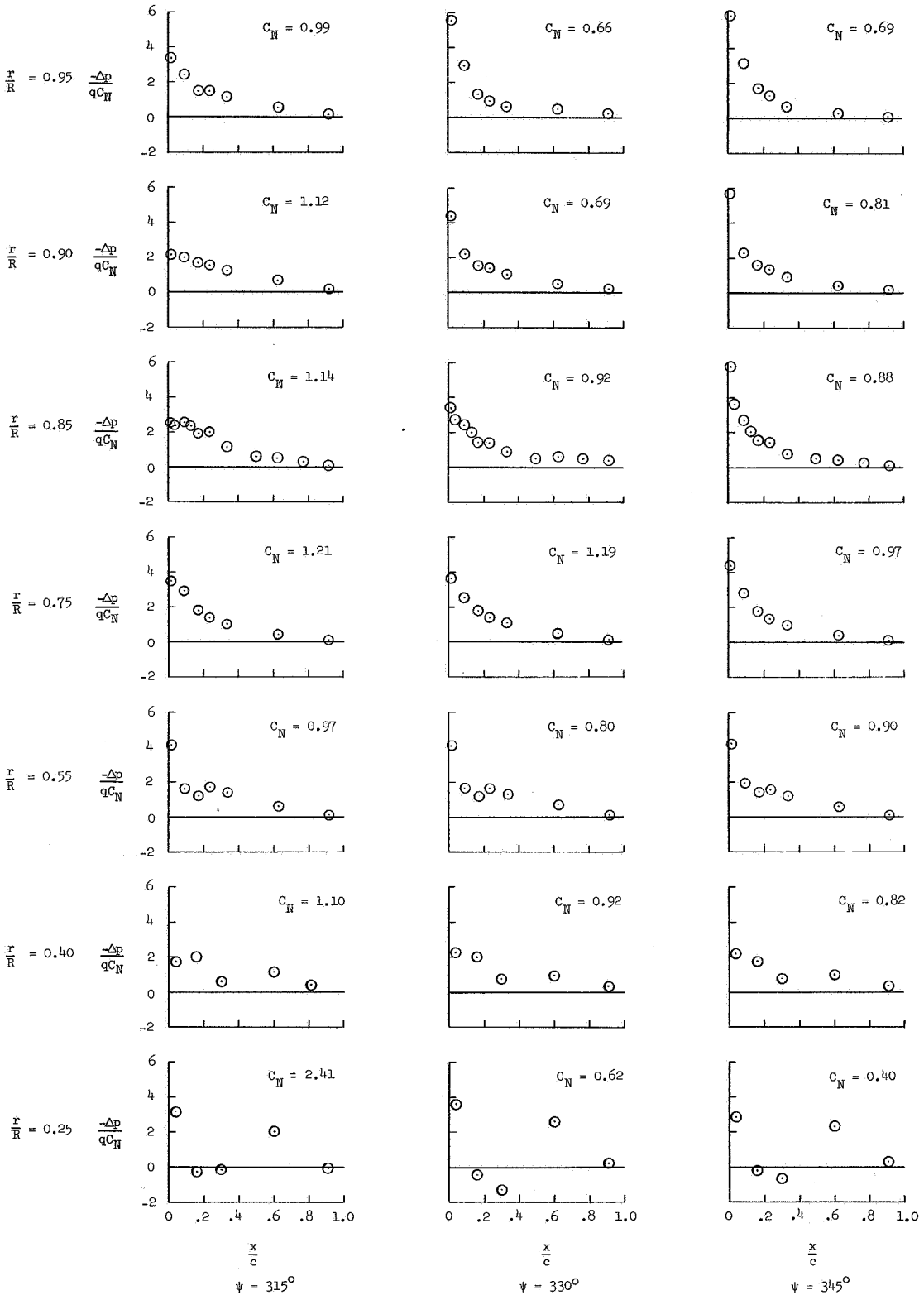

Figure 3.- Concluded.

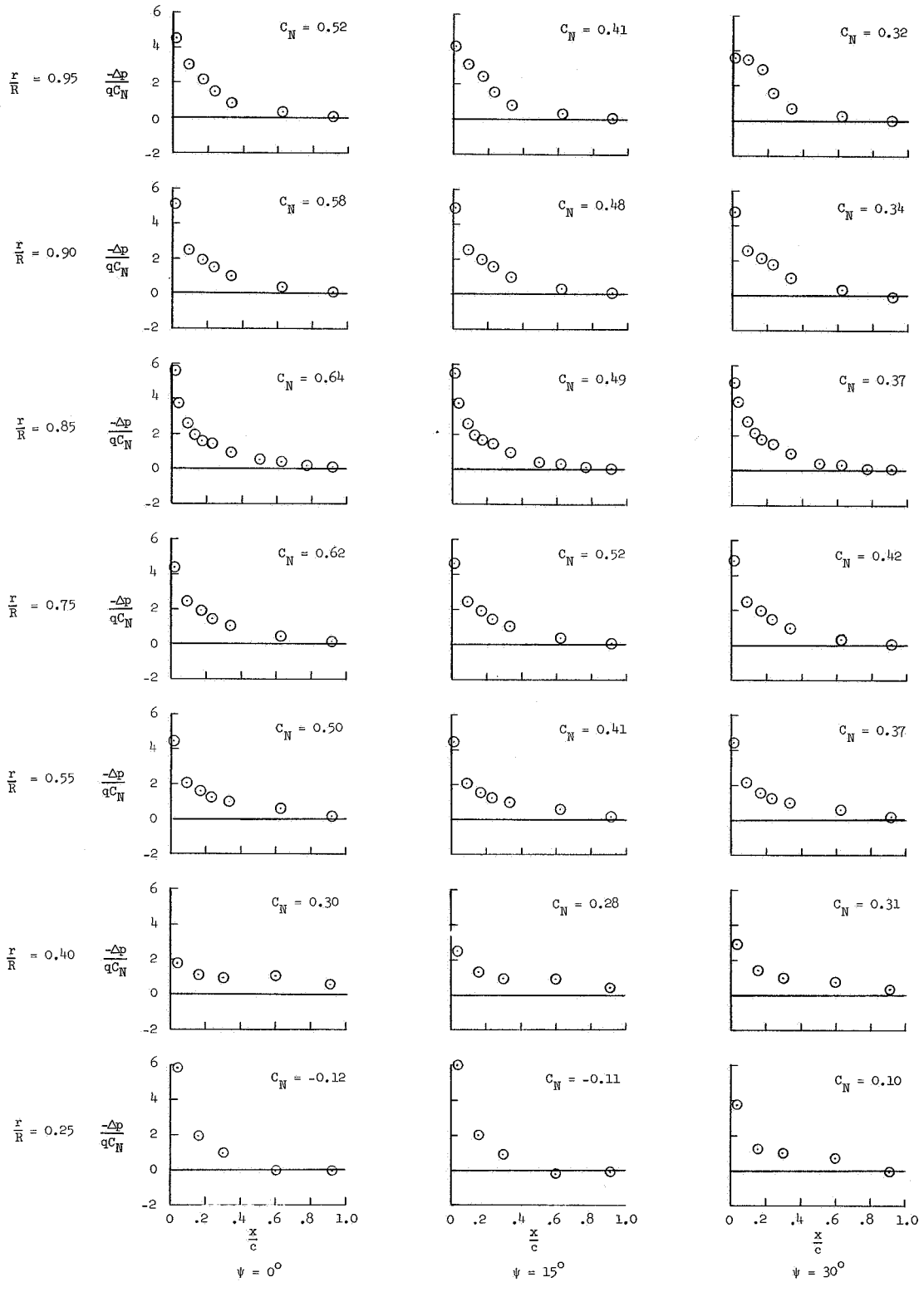

Figure 4.- Normalized chordwise pressure distributions for flight to obtain high blade Mach numbers.

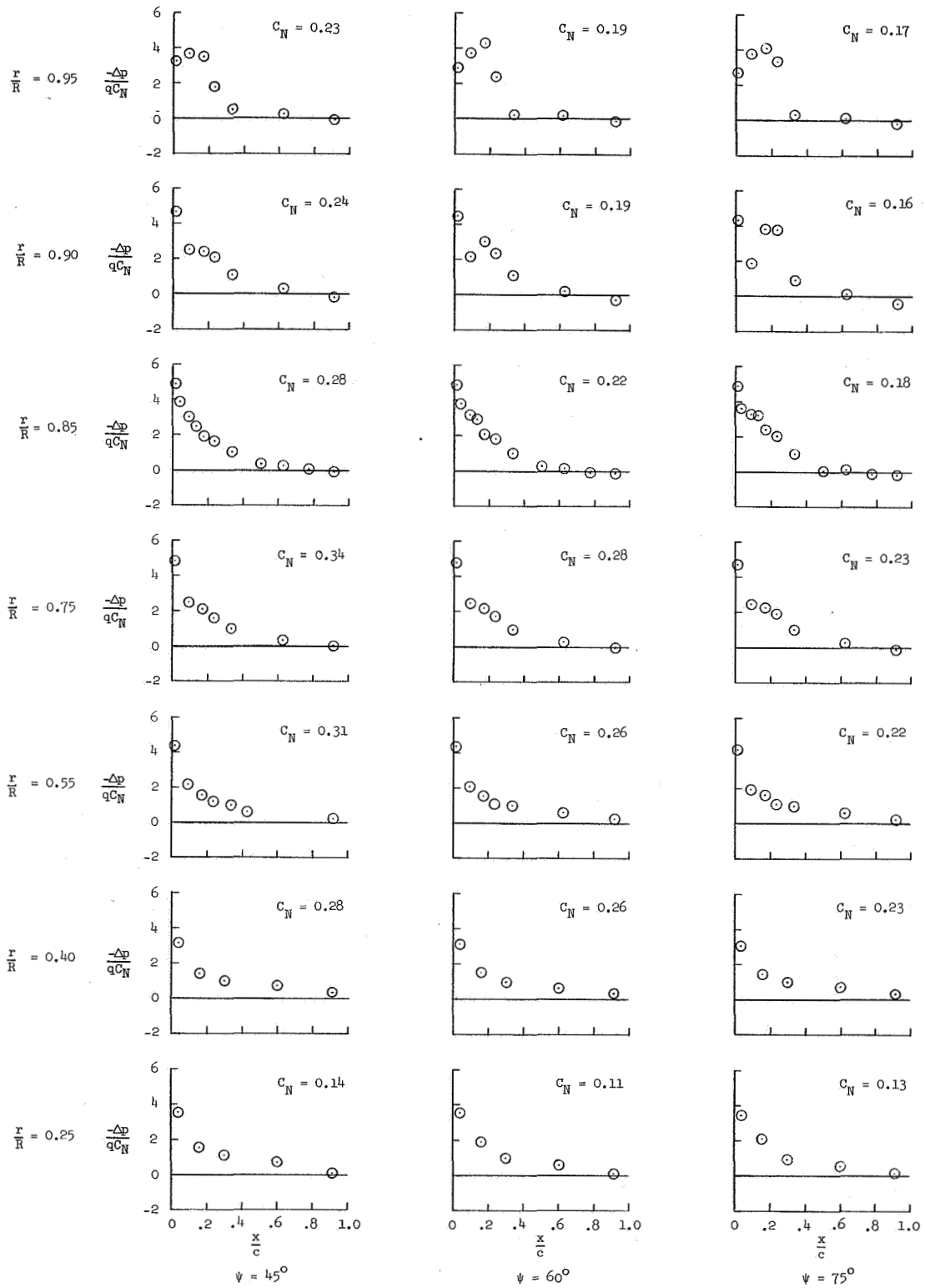

Figure 4.- Continued.

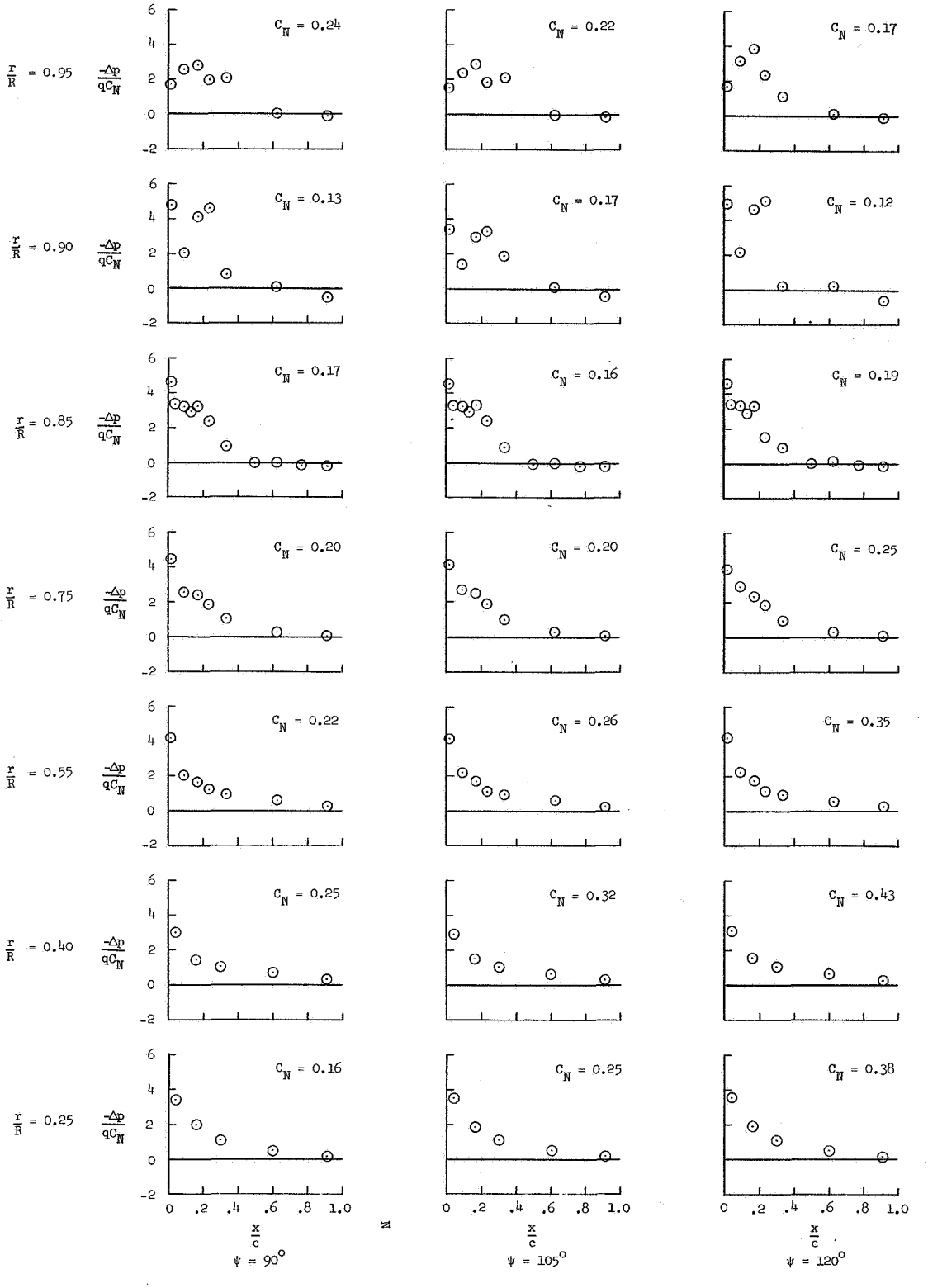

Figure 4.- Continued.

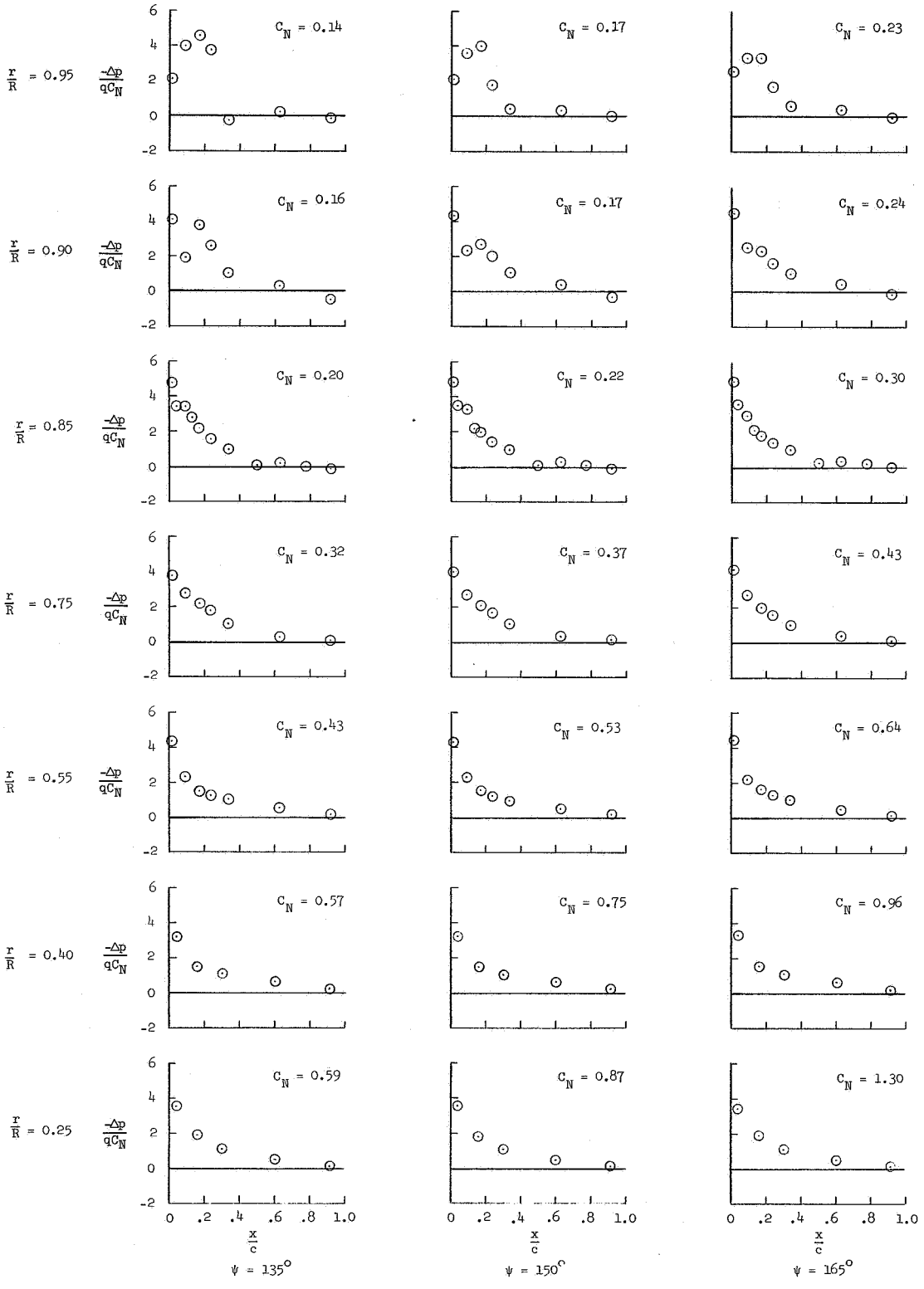

Figure 4.- Continued.

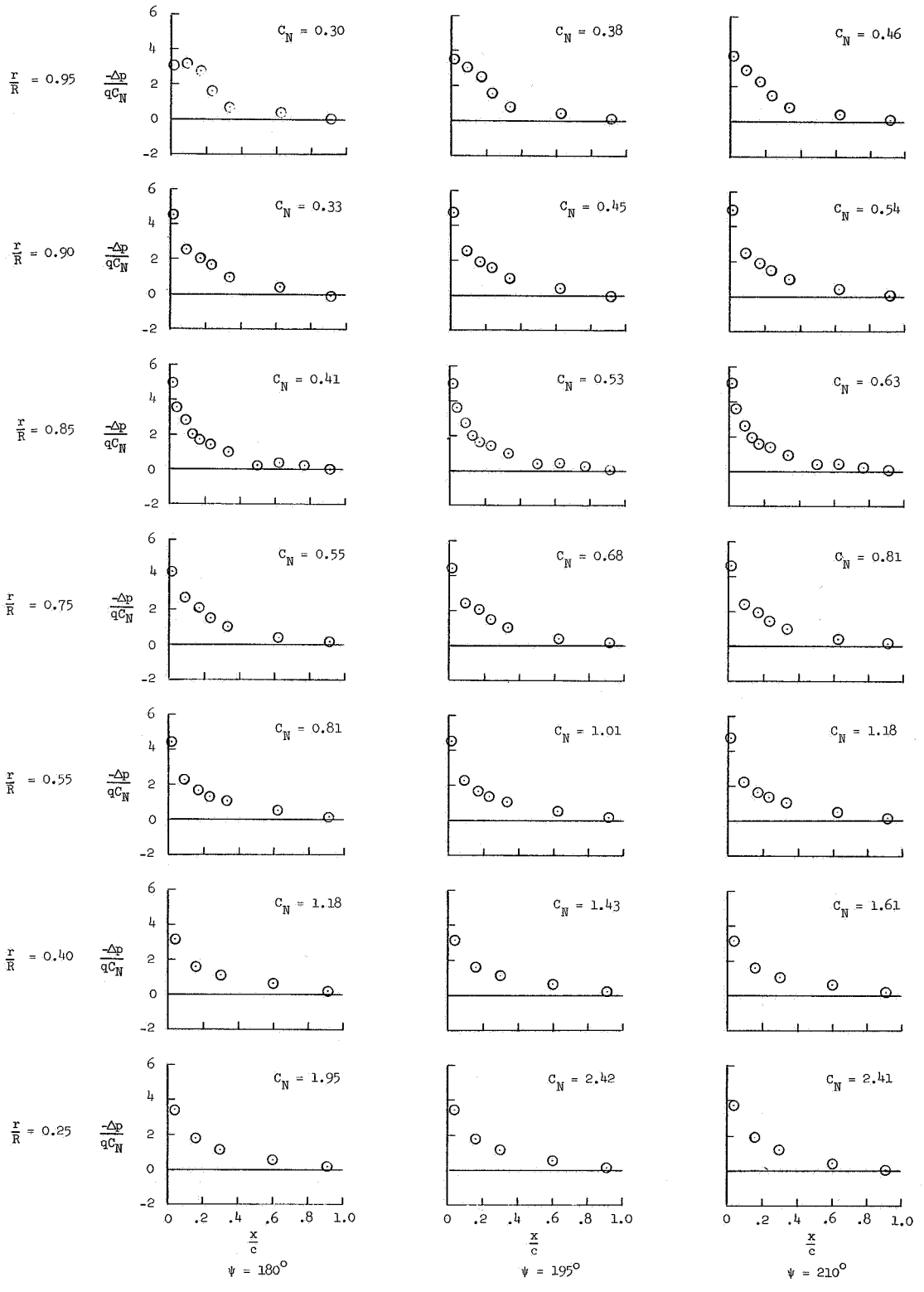

Figure 4.- Continued.

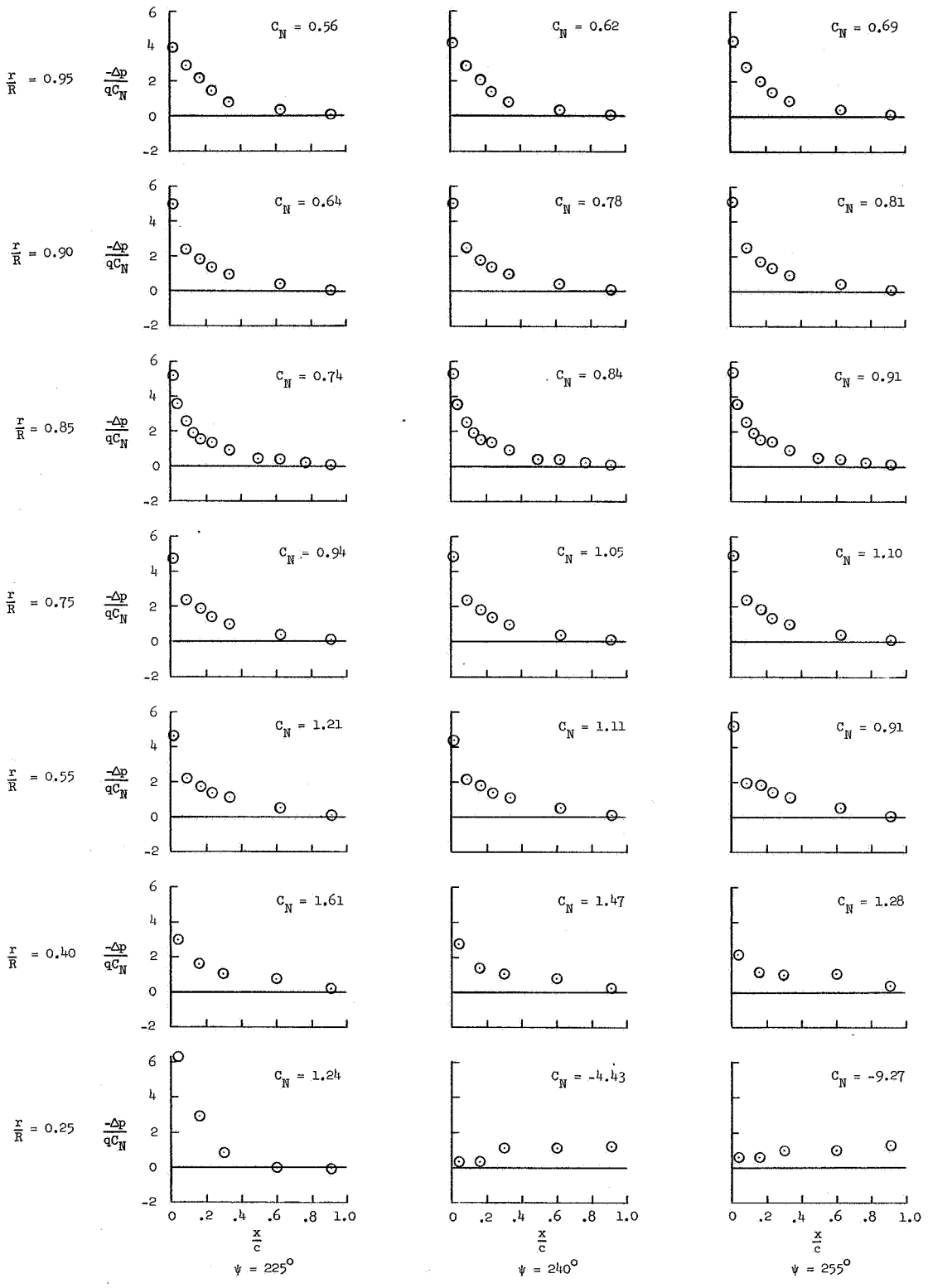

Figure 4.- Continued.

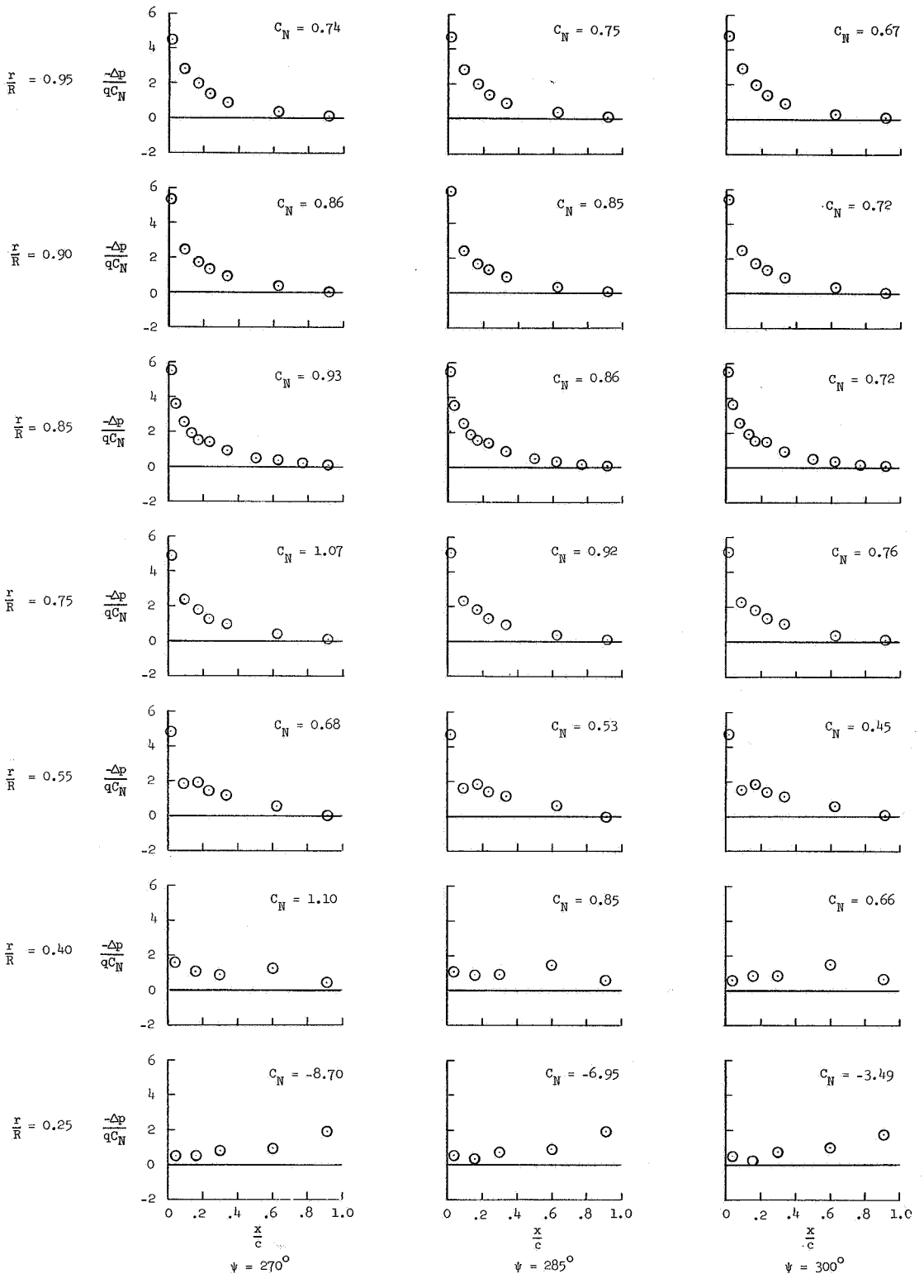

Figure 4.- Continued.

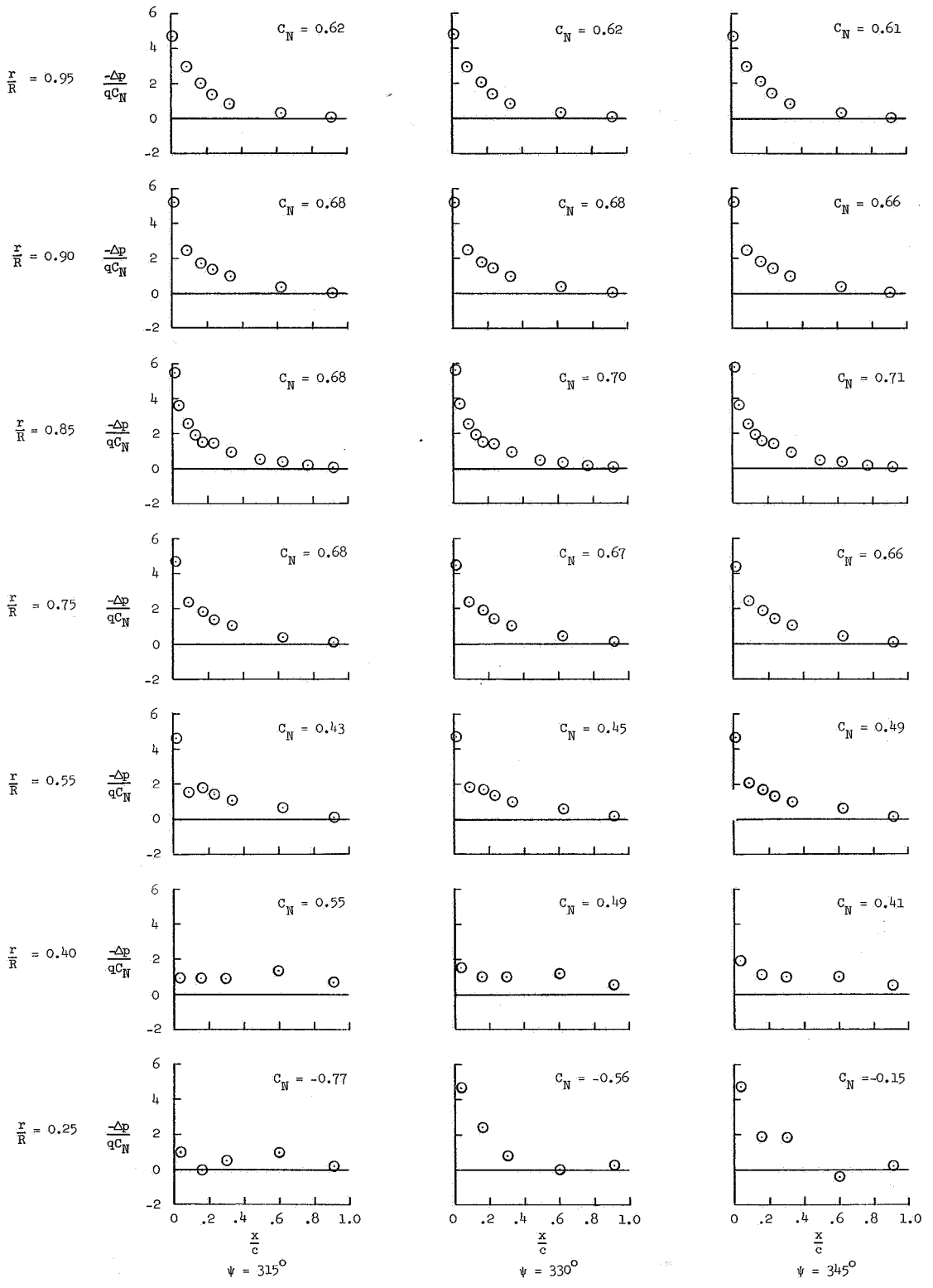

Figure 4.- Concluded.

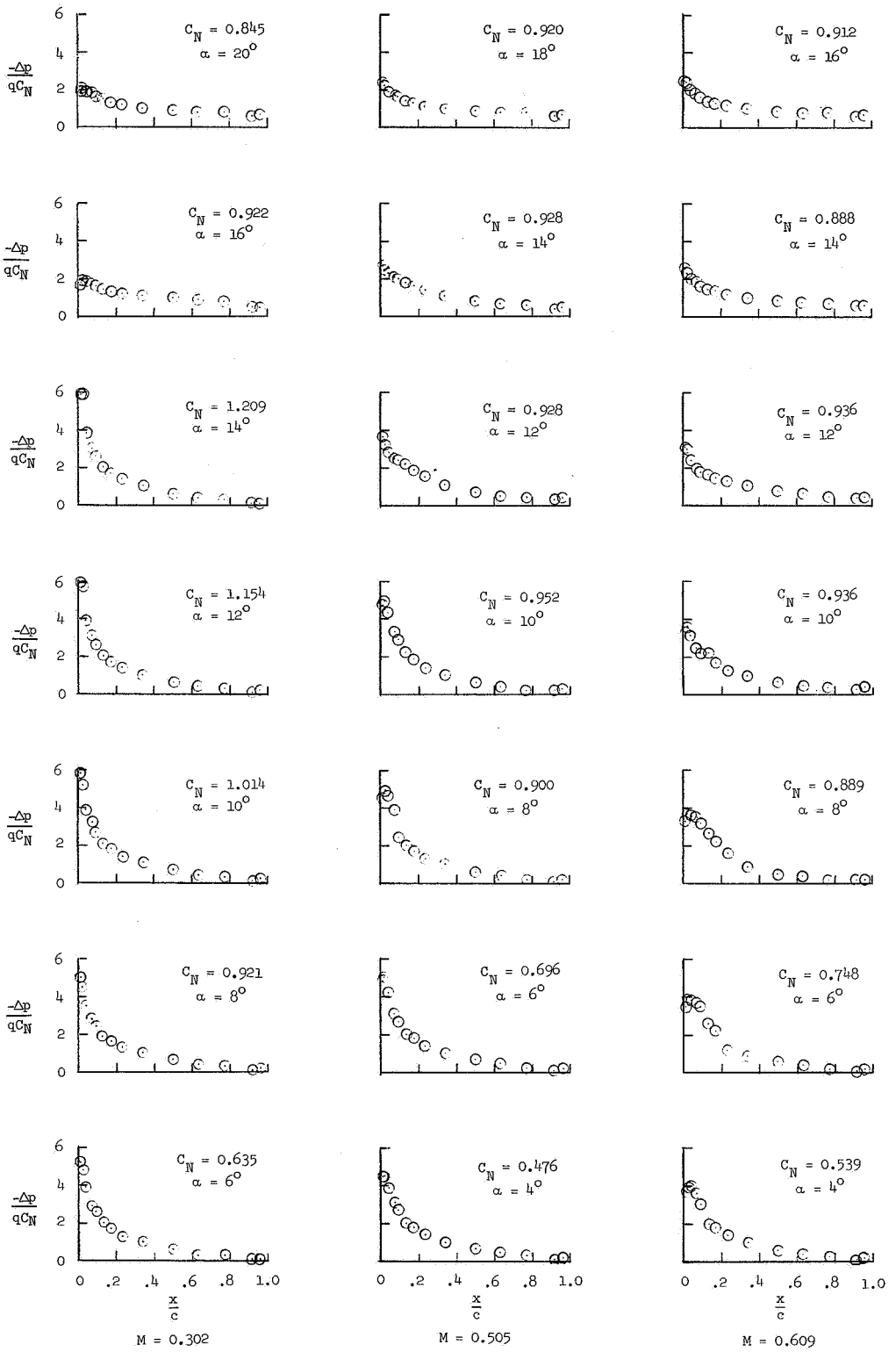

Figure 5.- Normalized chordwise static two-dimensional airfoil characteristics from reference 5. The indicated Mach numbers are mean corrected values for the angles of attack shown.

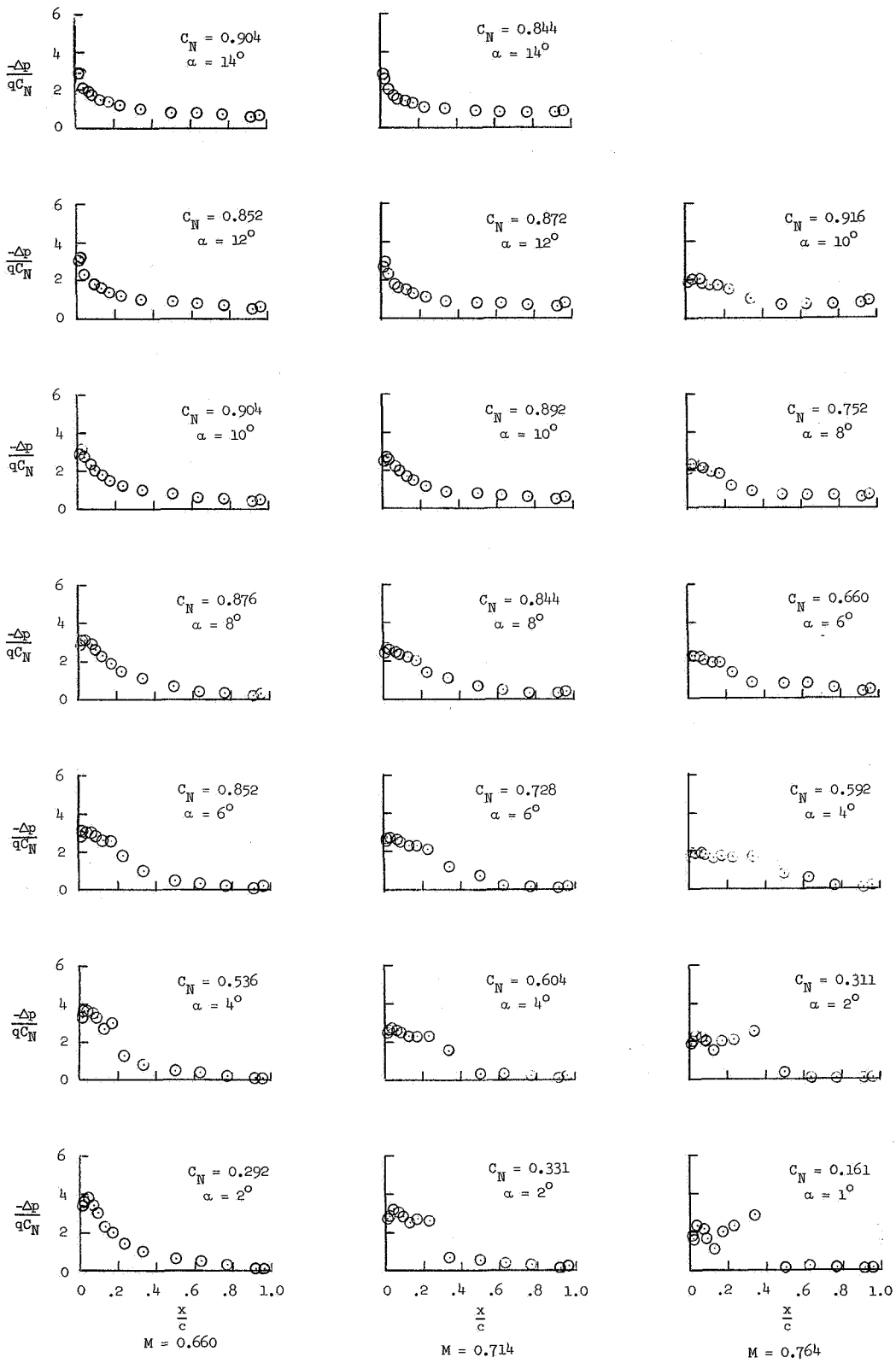

Figure 5.- Concluded.

○ Point where comparison showed agreement between flight and two-dimensional distributions (see fig. 11)

● Point where comparison showed disagreement between flight and two-dimensional distributions (see fig. 11)

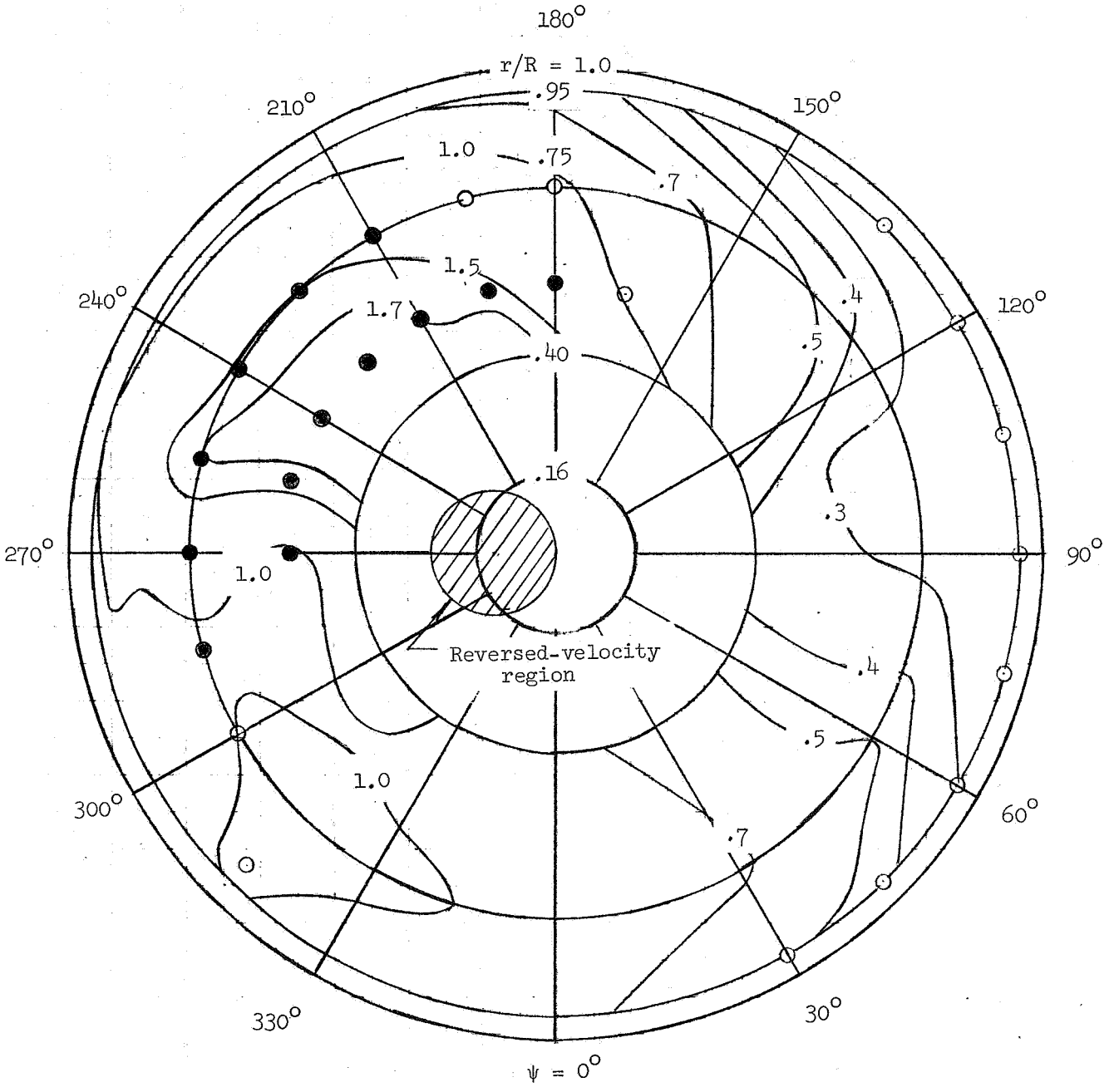

Figure 6.- Local normal-force coefficients for flight to obtain blade stall.

○ Point where comparison showed agreement between flight and two-dimensional distributions (see fig. 12)

● Point where comparison showed disagreement between flight and two-dimensional distributions (see fig. 12)

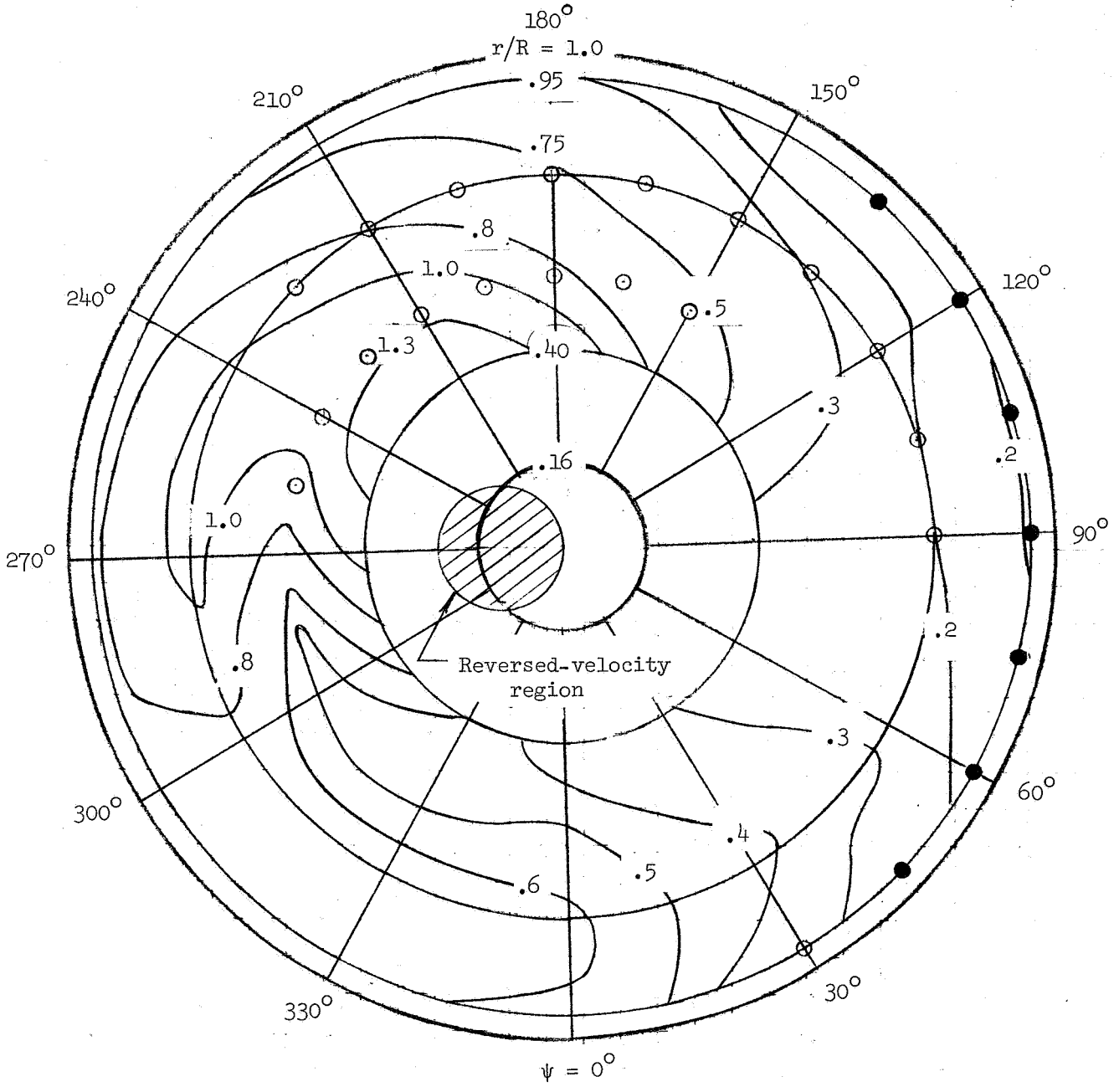

Figure 7.- Local normal-force coefficients for flight to obtain high blade Mach numbers.

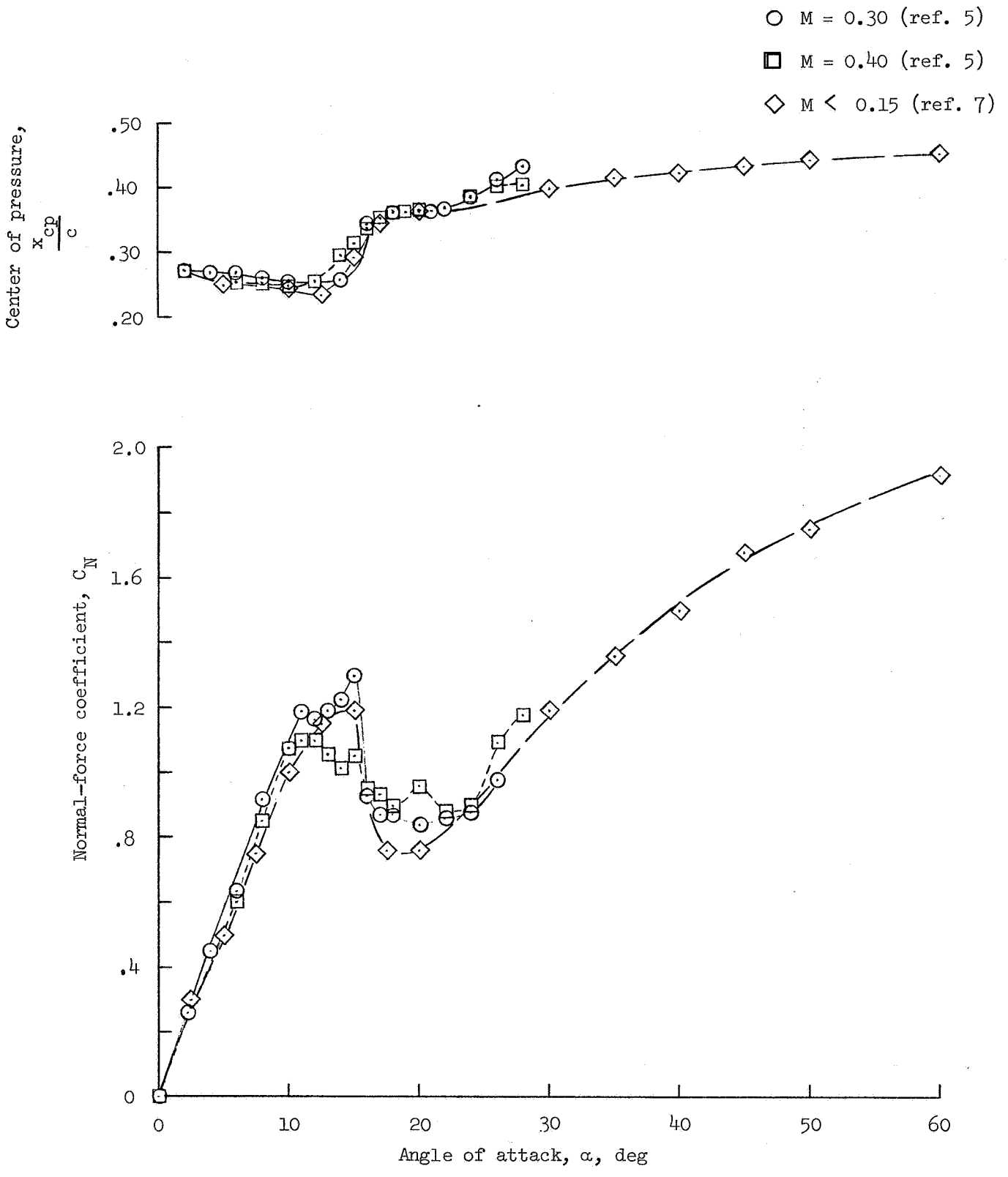

Figure 8.- Two-dimensional airfoil characteristics of a modified (ref. 5) and standard (ref. 7) NACA 0012 airfoil at various Mach numbers.

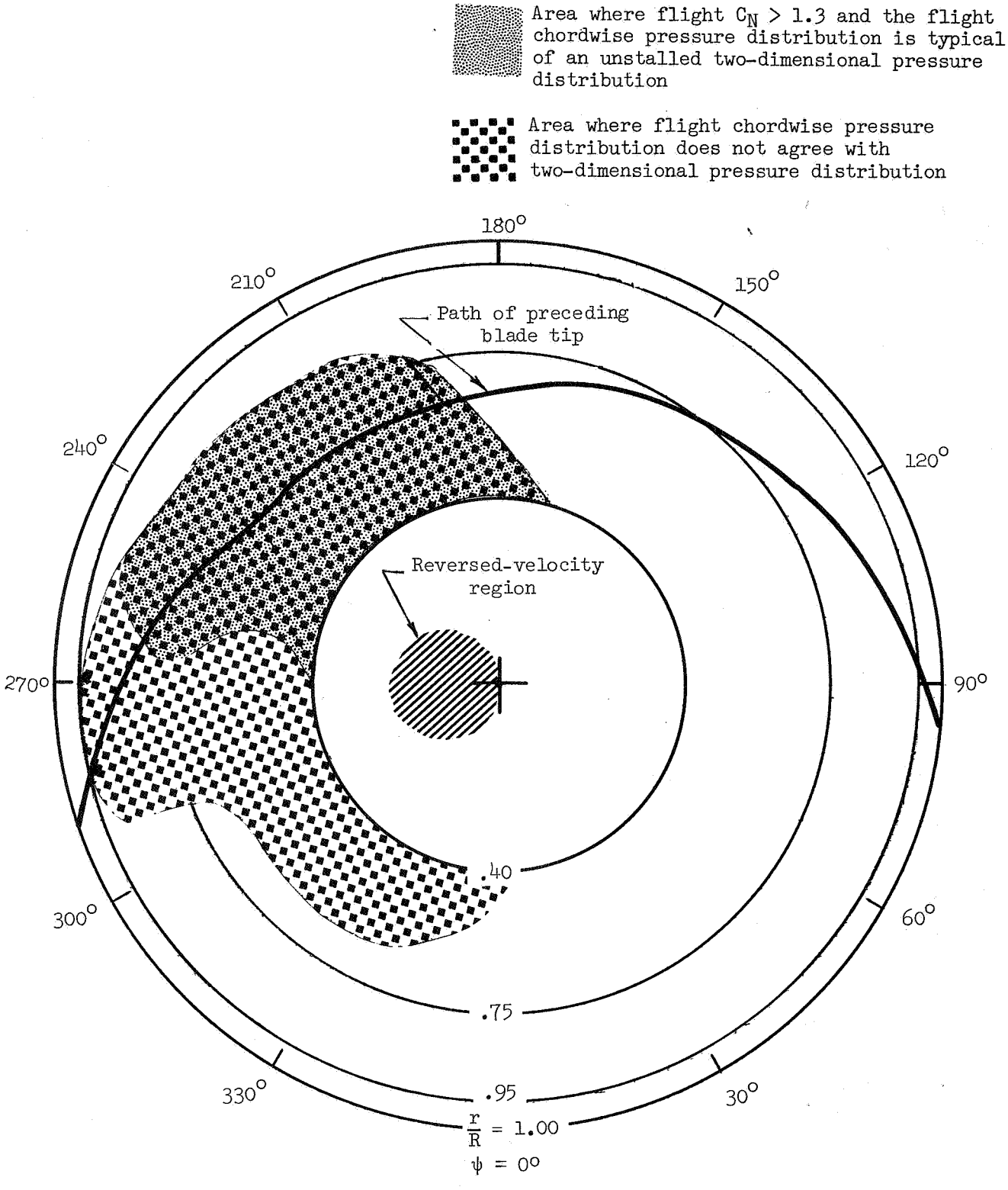

Figure 9.- Areas on the rotor disk where $C_N > 1.3$ and areas where flight and two-dimensional pressure distributions did not agree for flight to obtain blade stall.

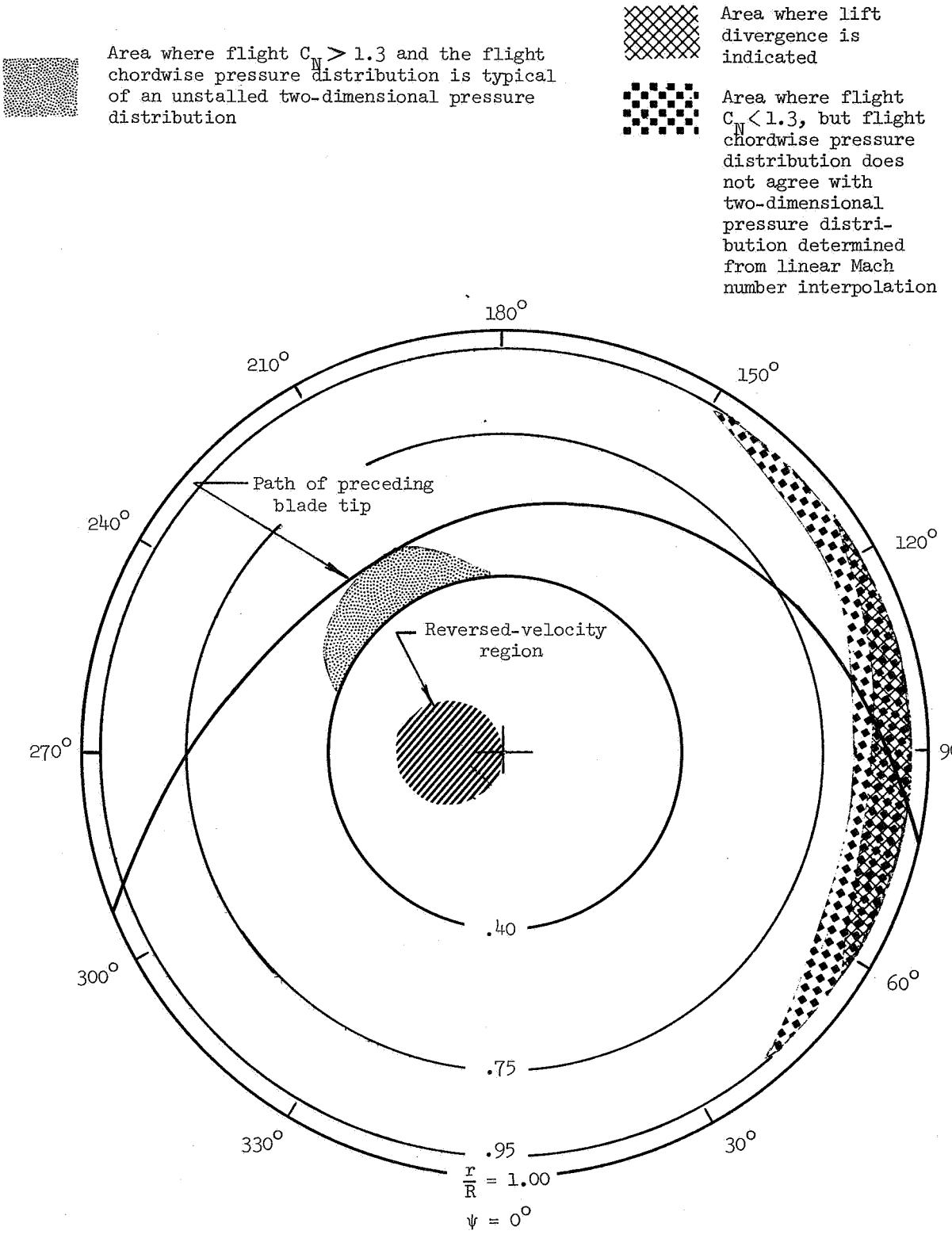

Figure 10.- Areas on the rotor disk where flight and two-dimensional pressure distributions did not agree for flight to obtain high Mach numbers.

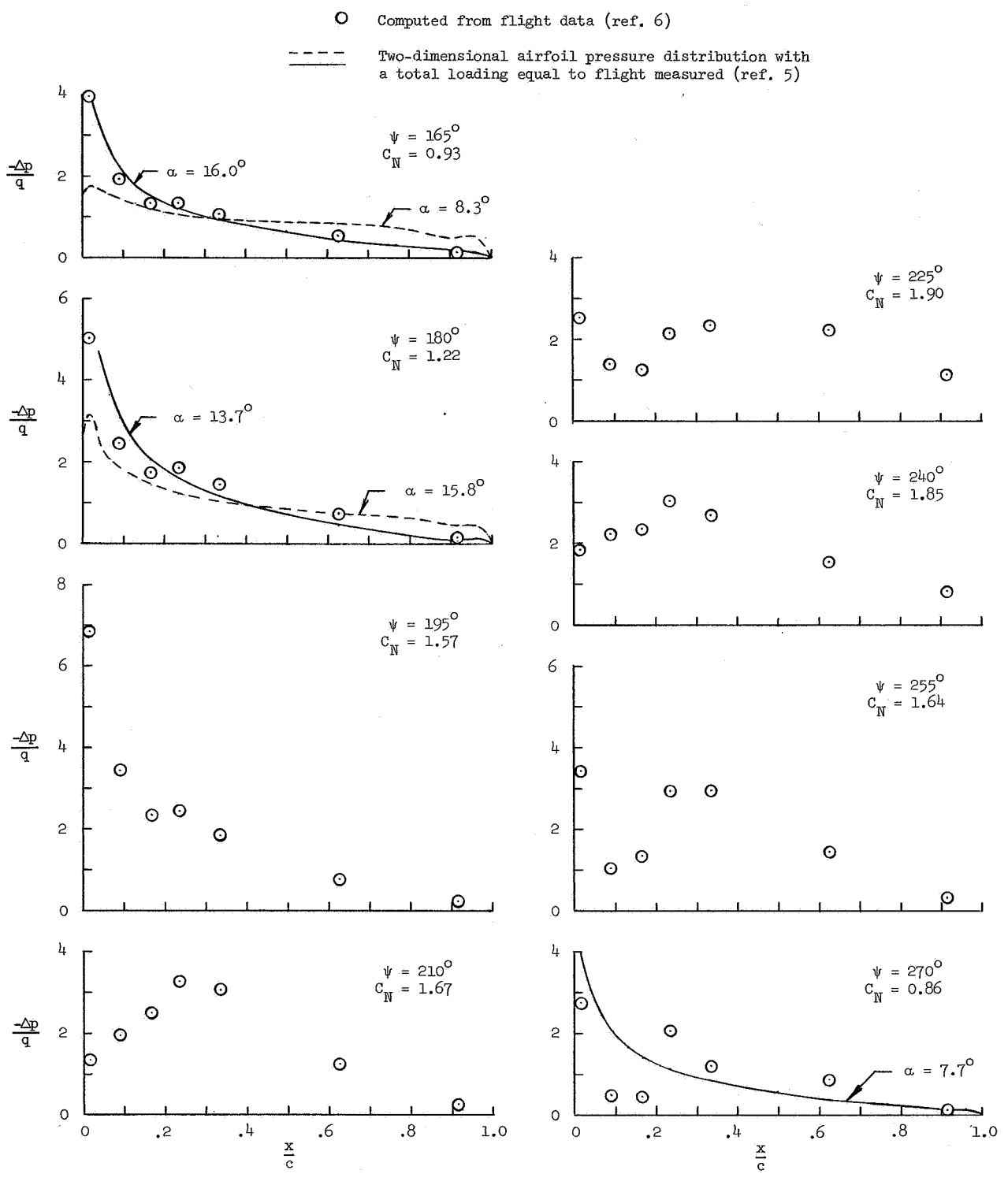

(a) $\frac{r}{R} = 0.55$.

Figure 11.- Chordwise pressure distributions for flight to obtain blade stall. Comparison with two-dimensional data is made when possible.

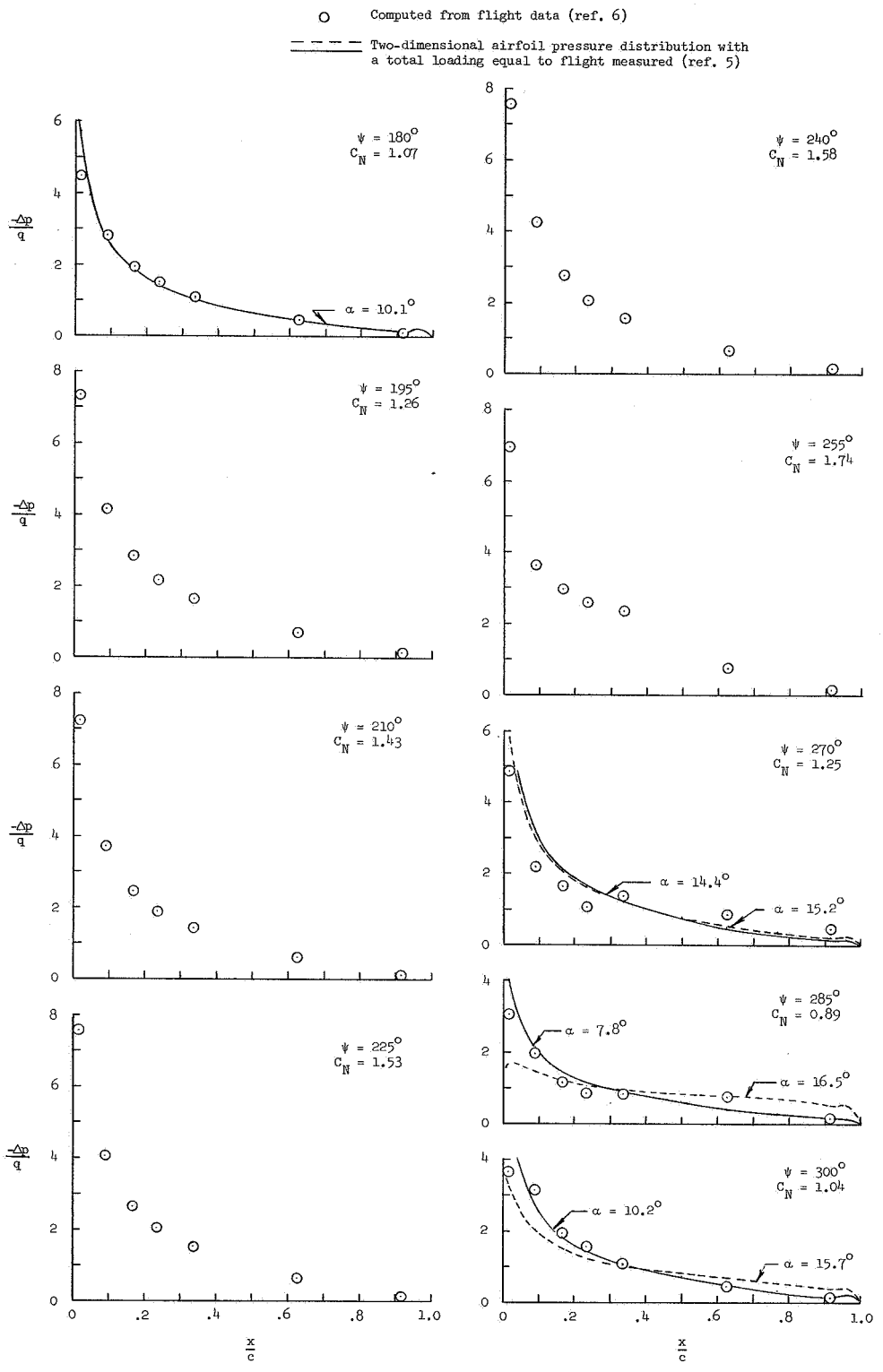

(b) $\frac{r}{R} = 0.75$.

Figure 11.- Continued.

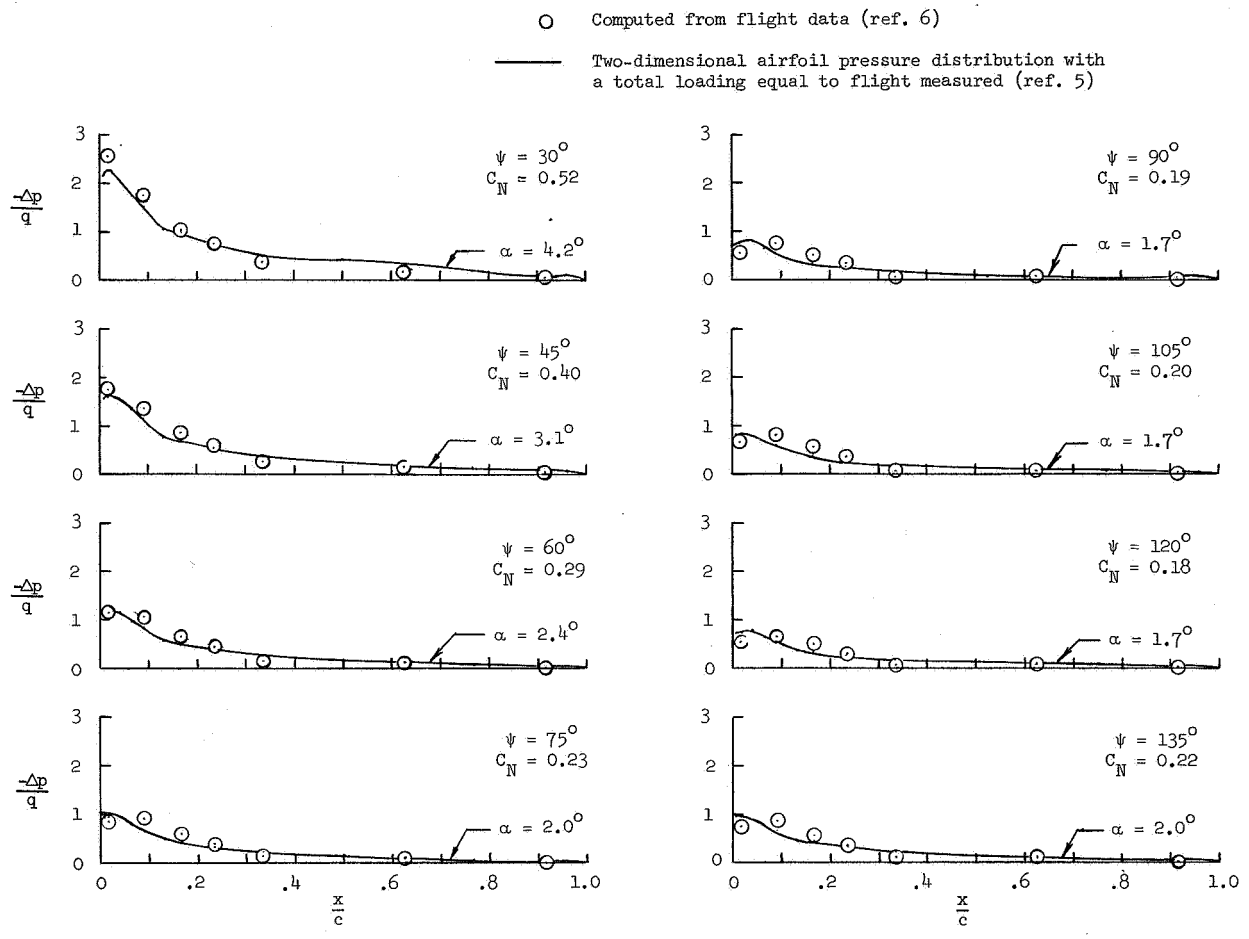

(c) $\frac{r}{R} = 0.95$.

Figure 11.- Continued.

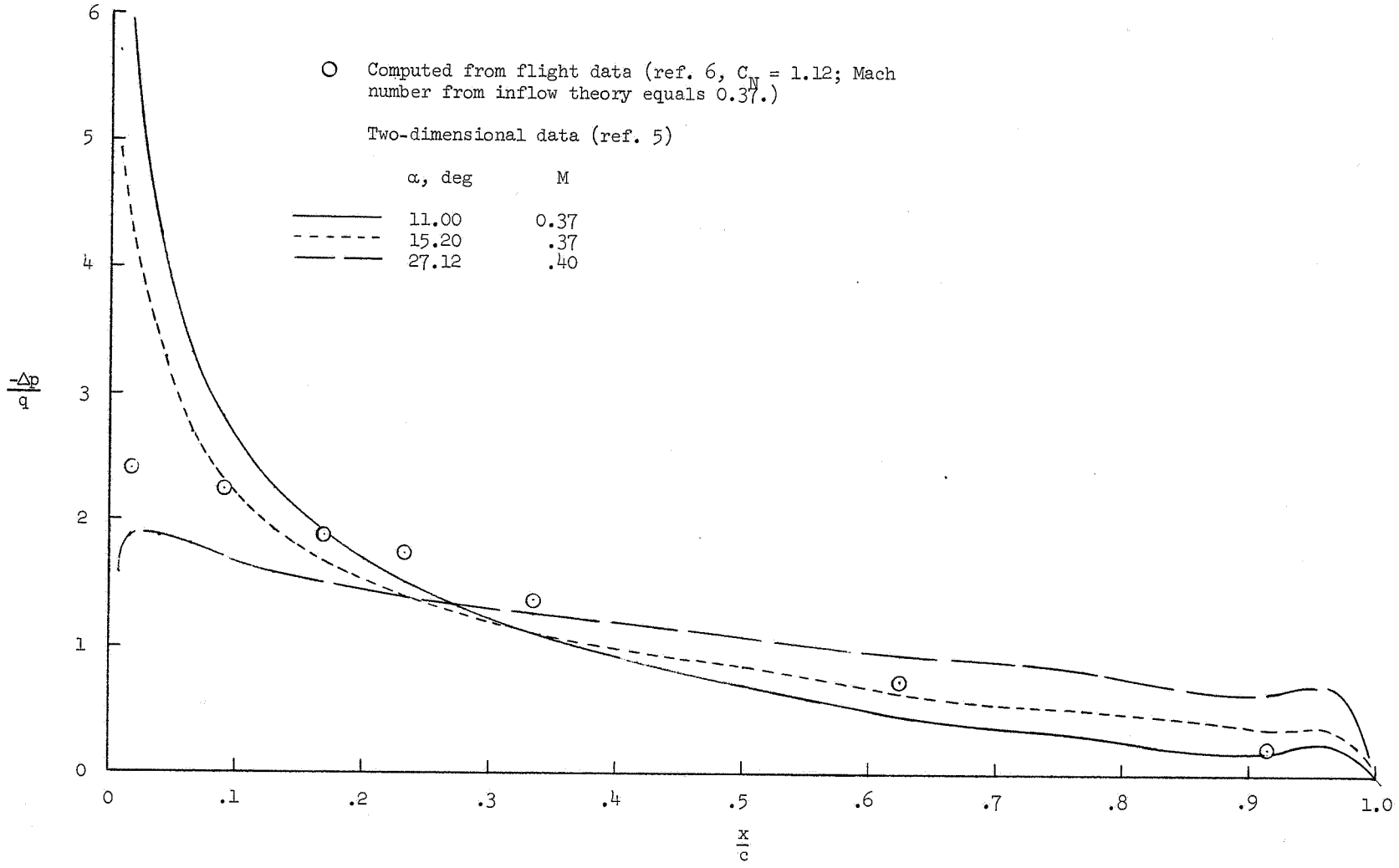

(d) $\psi = 315^0$; $\frac{r}{R} = 0.90$.

Figure 11.- Concluded.

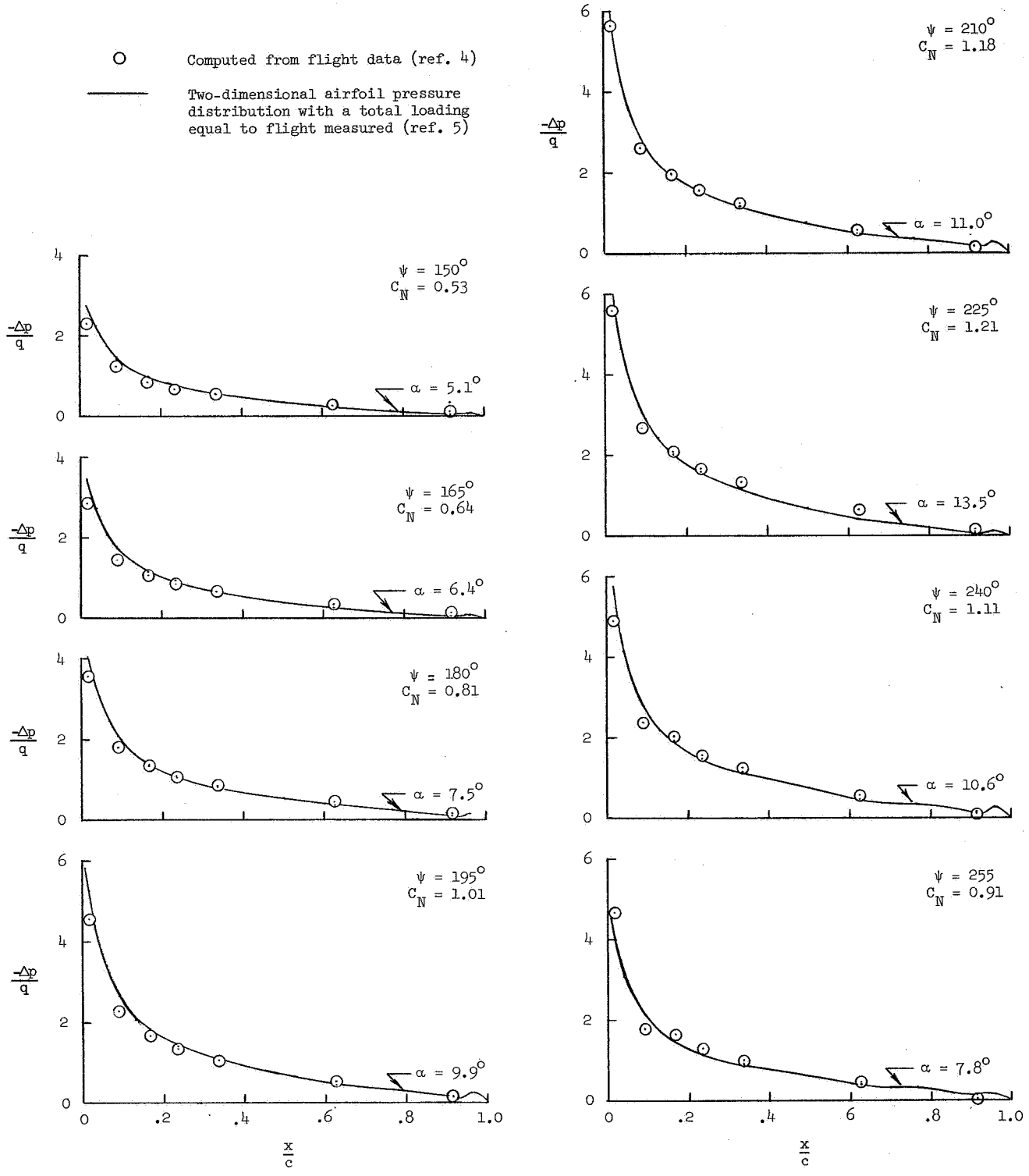

(a) $\frac{r}{R} = 0.55$.

Figure 12.- Chordwise pressure distributions for flight to obtain high blade Mach numbers. Comparison with two-dimensional data is made when possible.

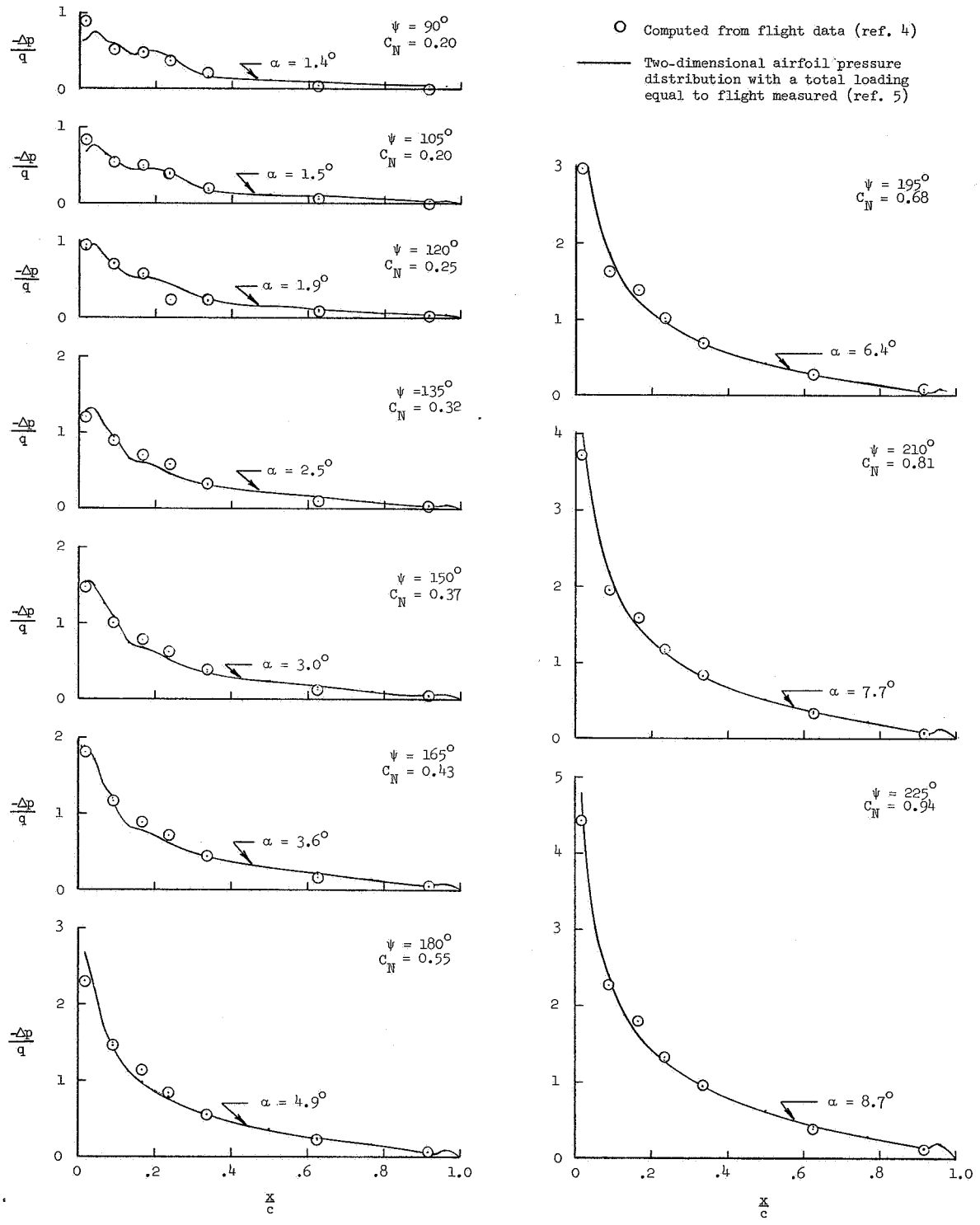

(b) $\frac{r}{R} = 0.75$.

Figure 12.- Continued.

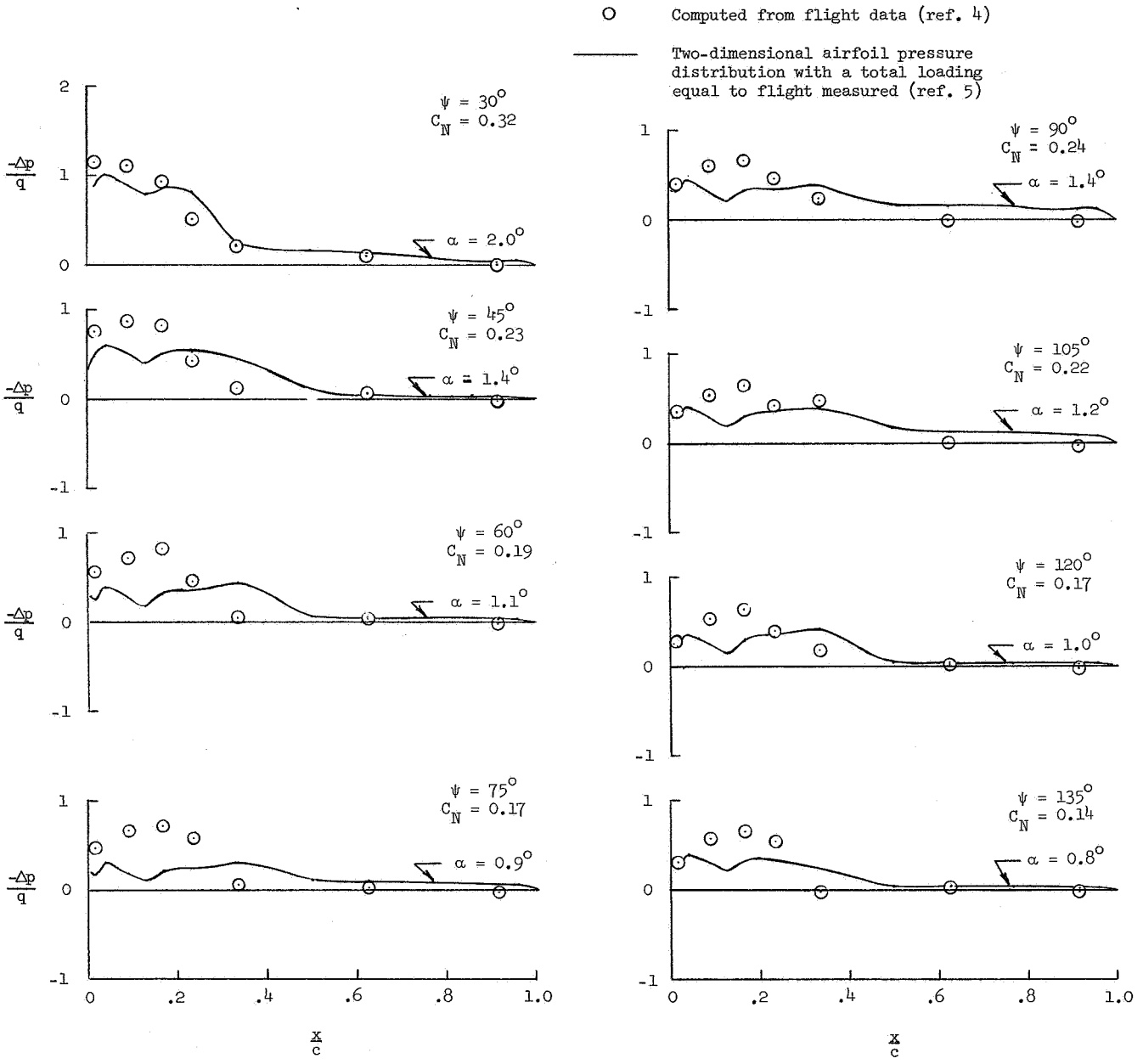

(c) $\frac{r}{R} = 0.95$.

Figure 12.- Concluded.

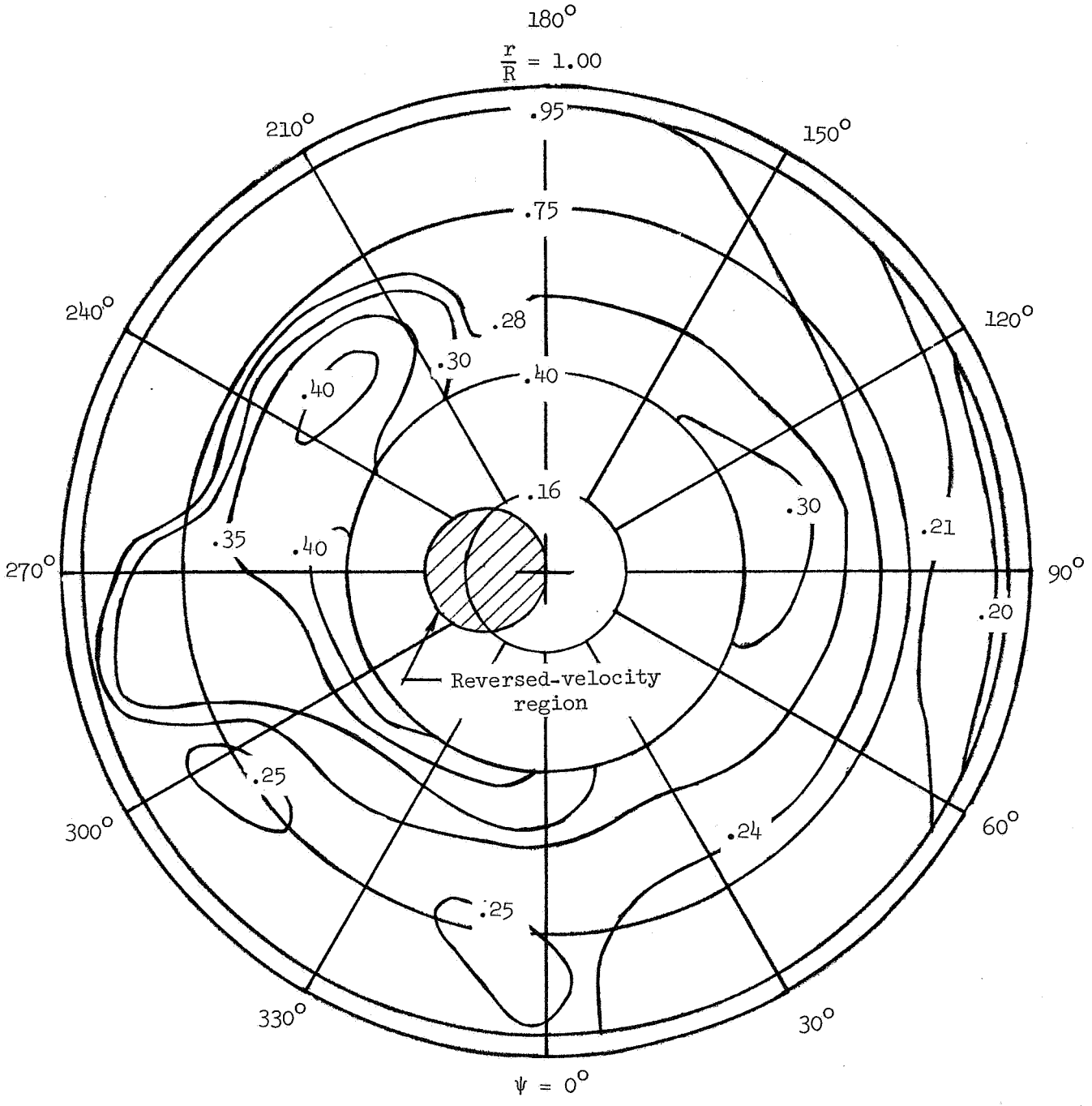

(a) Lines of constant centers of pressure.

Figure 13.- Contour plots showing centers of pressure for flight to obtain blade stall.

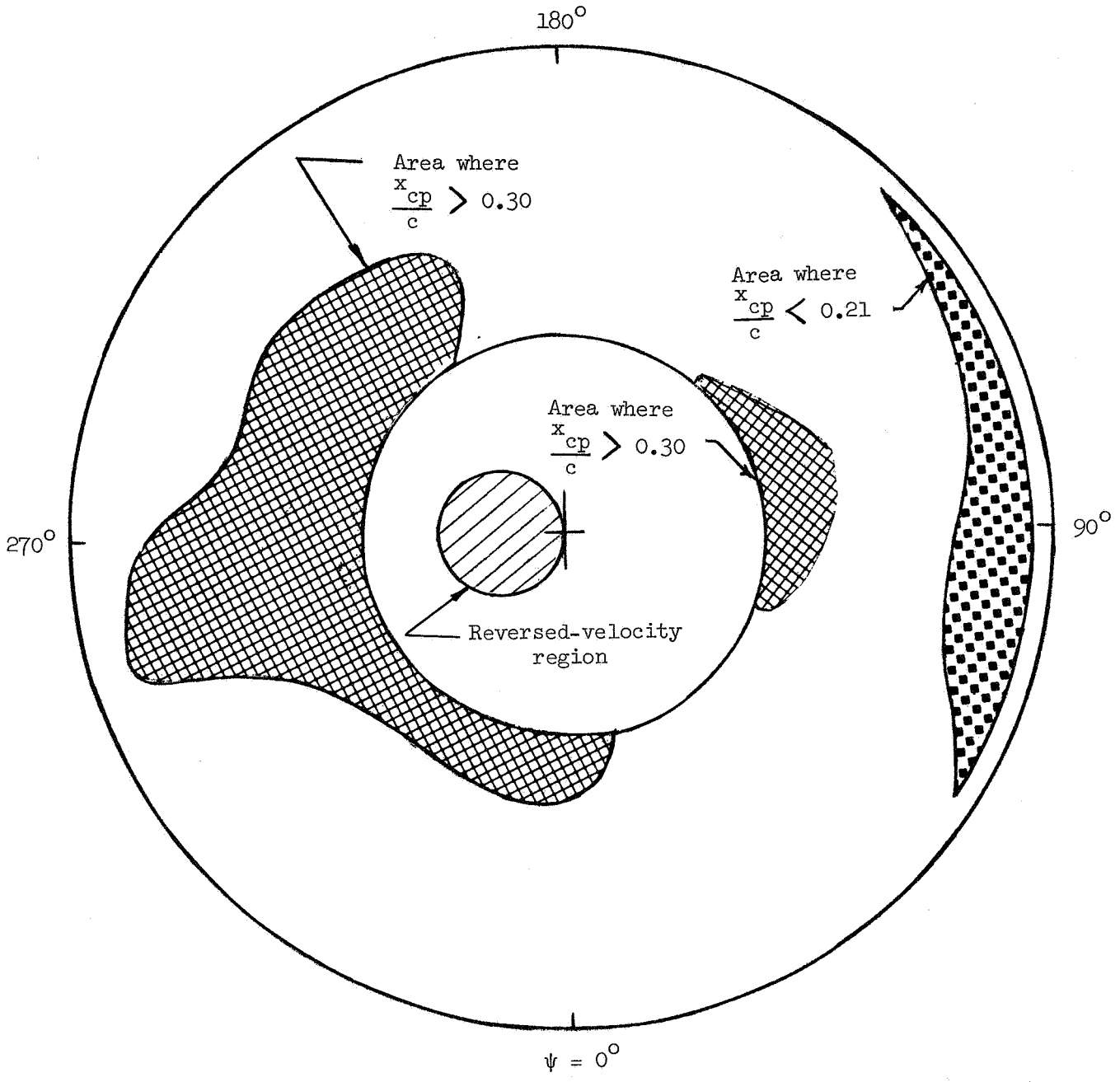

(b) Center-of-pressure areas forward of 21-percent-chord point and aft of 30-percent-chord point.

Figure 13.- Concluded.

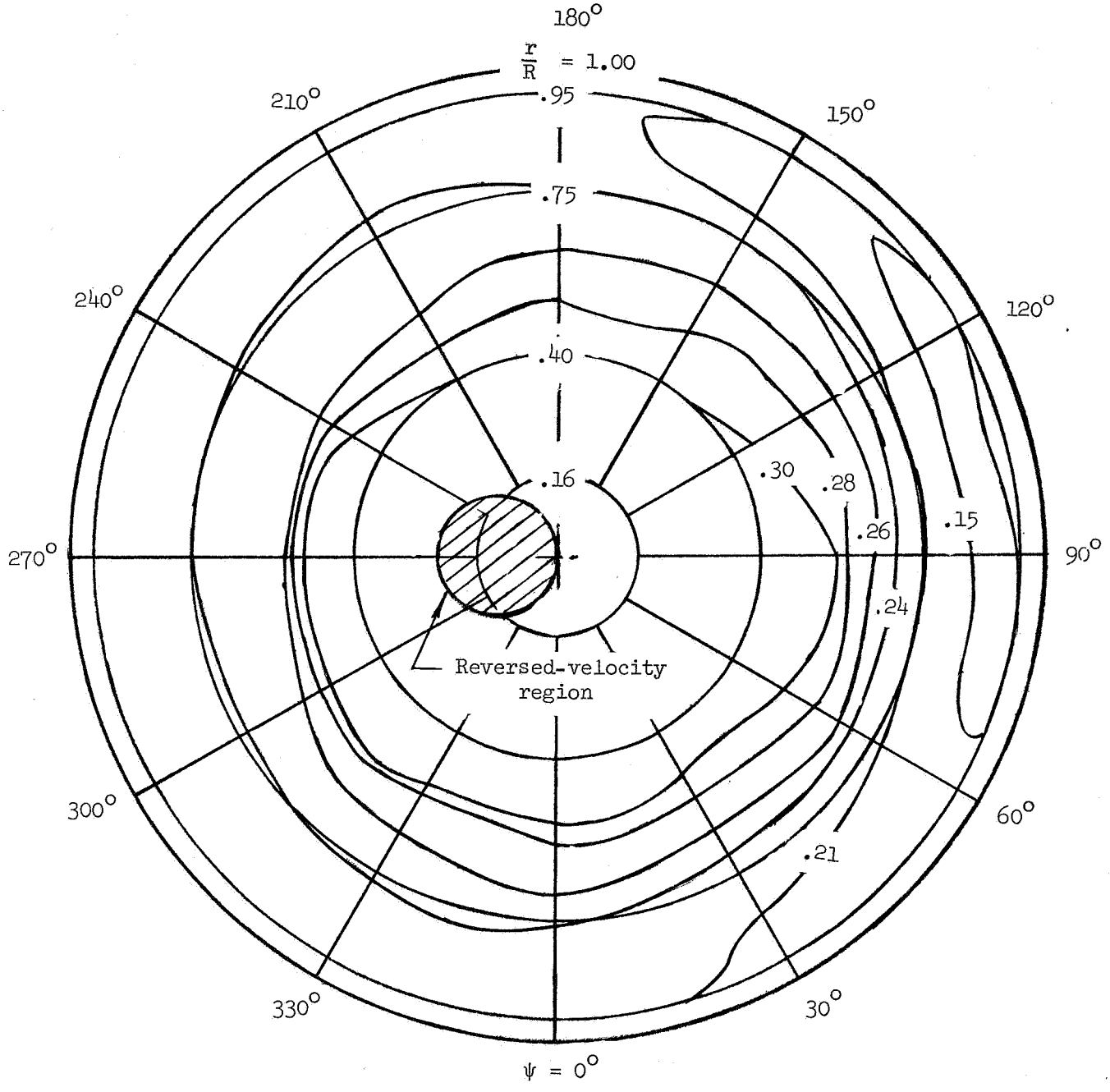

(a) Lines of constant centers of pressure.

Figure 14.- Contour plots showing centers of pressure for flight to obtain high blade Mach numbers.

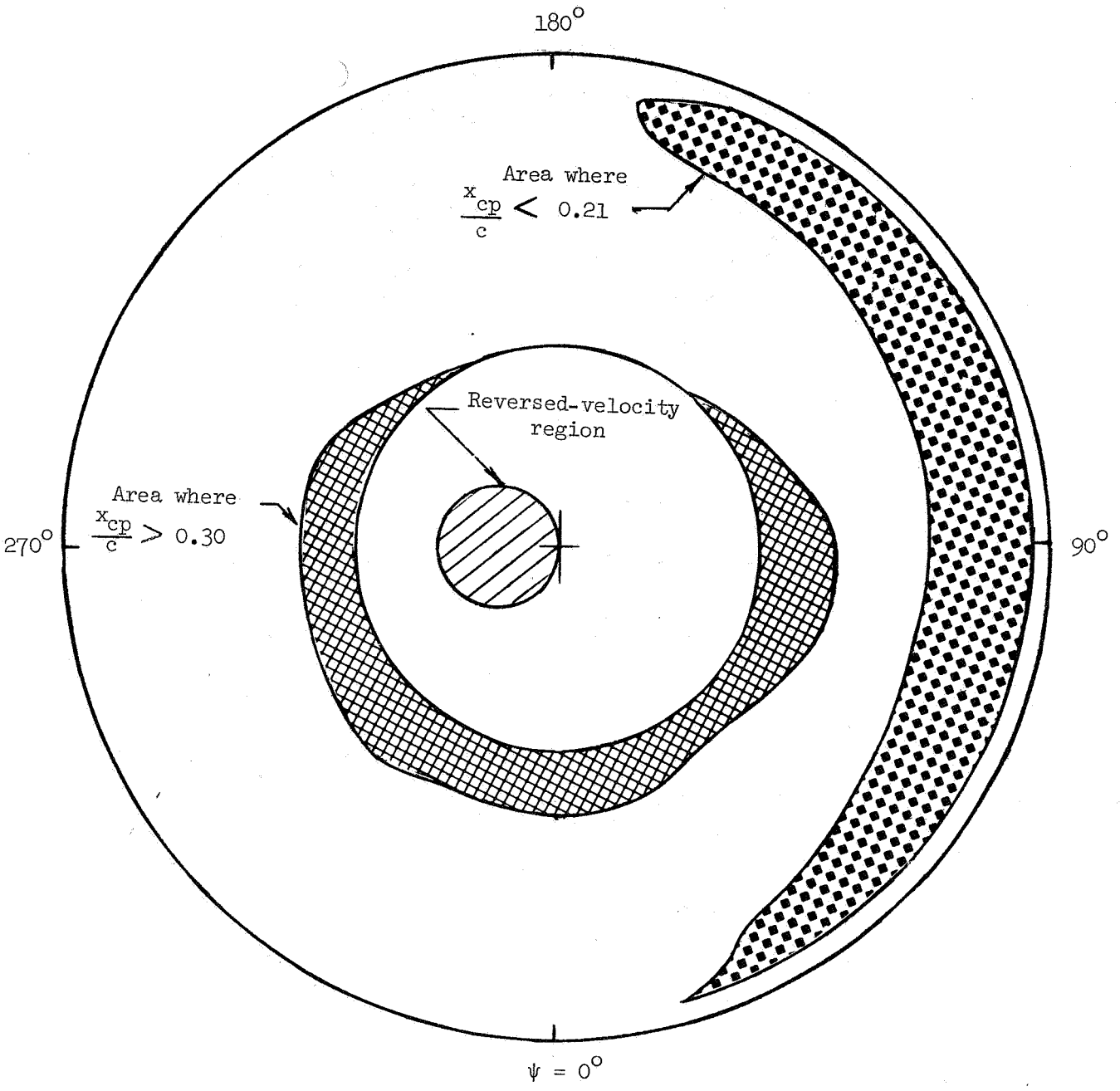

(b) Center-of-pressure areas forward of 21-percent-chord point and aft of 30-percent-chord point.

Figure 14.- Concluded.

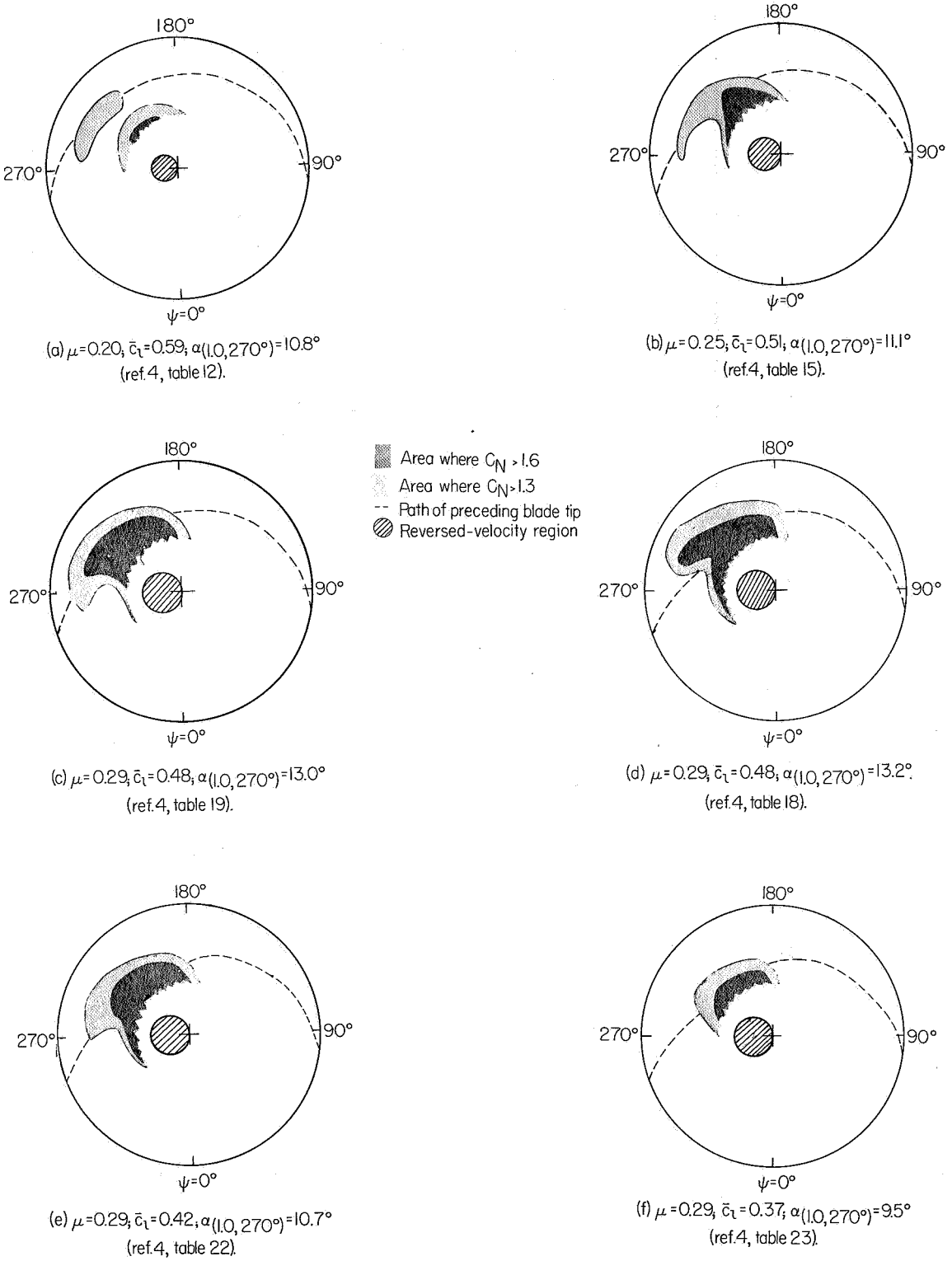

(a) μ=0.20; $\bar{c}_l$=0.59; $\alpha_{(1.0,270°)}$=10.8° (ref. 4, table 12).

(b) μ=0.25; $\bar{c}_l$=0.51; $\alpha_{(1.0,270°)}$=11.1° (ref. 4, table 15).

(c) μ=0.29; $\bar{c}_l$=0.48; $\alpha_{(1.0,270°)}$=13.0° (ref. 4, table 19).

(d) μ=0.29; $\bar{c}_l$=0.48; $\alpha_{(1.0,270°)}$=13.2° (ref. 4, table 18).

(e) μ=0.29; $\bar{c}_l$=0.42; $\alpha_{(1.0,270°)}$=10.7° (ref. 4, table 22).

(f) μ=0.29; $\bar{c}_l$=0.37; $\alpha_{(1.0,270°)}$=9.5° (ref. 4, table 23).

Figure 15.- Areas on the rotor where the flight normal-force coefficients are greater than the two-dimensional stall value (C_N = 1.3) for several trim-level-flight conditions.

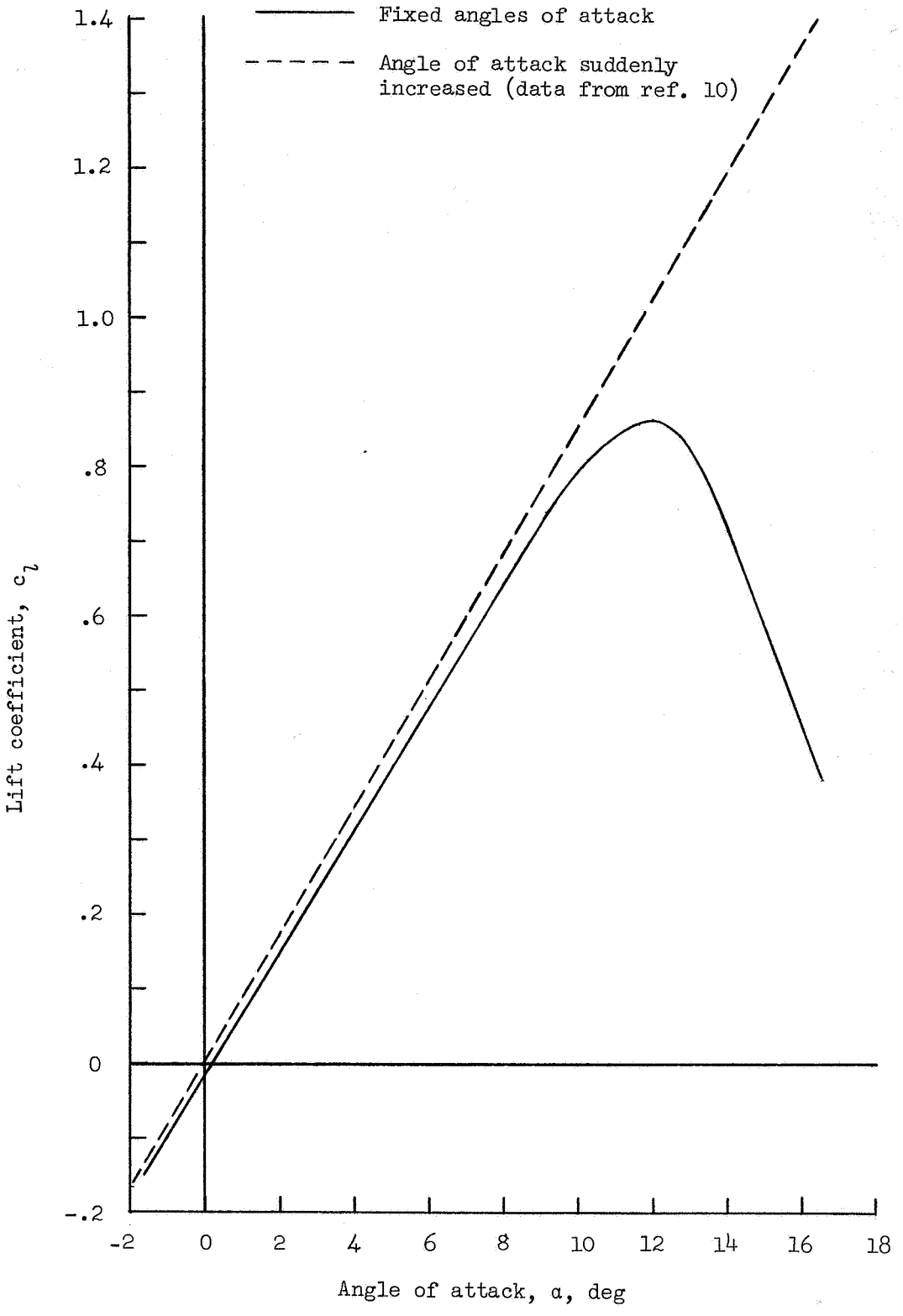

Figure 16.- Lift curves for an airfoil tested statically at fixed angles of attack and for an airfoil for which the angle of attack was suddenly increased.

NASA-Langley, 1967 —— 2

10-5-67

"The aeronautical and space activities of the United States shall be conducted so as to contribute . . . to the expansion of human knowledge of phenomena in the atmosphere and space. The Administration shall provide for the widest practicable and appropriate dissemination of information concerning its activities and the results thereof."

—NATIONAL AERONAUTICS AND SPACE ACT OF 1958

NASA SCIENTIFIC AND TECHNICAL PUBLICATIONS

TECHNICAL REPORTS: Scientific and technical information considered important, complete, and a lasting contribution to existing knowledge.

TECHNICAL NOTES: Information less broad in scope but nevertheless of importance as a contribution to existing knowledge.

TECHNICAL MEMORANDUMS: Information receiving limited distribution because of preliminary data, security classification, or other reasons.

CONTRACTOR REPORTS: Scientific and technical information generated under a NASA contract or grant and considered an important contribution to existing knowledge.

TECHNICAL TRANSLATIONS: Information published in a foreign language considered to merit NASA distribution in English.

SPECIAL PUBLICATIONS: Information derived from or of value to NASA activities. Publications include conference proceedings, monographs, data compilations, handbooks, sourcebooks, and special bibliographies.

TECHNOLOGY UTILIZATION PUBLICATIONS: Information on technology used by NASA that may be of particular interest in commercial and other non-aerospace applications. Publications include Tech Briefs, Technology Utilization Reports and Notes, and Technology Surveys.

Details on the availability of these publications may be obtained from:

SCIENTIFIC AND TECHNICAL INFORMATION DIVISION

NATIONAL AERONAUTICS AND SPACE ADMINISTRATION

Washington, D.C. 20546